A Global LIS/OTD Climatology of Lightning Flash Extent Density

Michael Peterson[1], Douglas Mach[2], Dennis Buechler[3]

[1] ISR-2, Los Alamos National Laboratory, Los Alamos, New Mexico

[2]Science and Technology Institute, Universities Space Research Association, Huntsville, AL, USA

[3]Department of Atmospheric Science, Information Technology & Systems Center, Earth System Science Center, University of Alabama in Huntsville, Huntsville, AL, USA

Corresponding author: Michael Peterson (mpeterson@lanl.gov), B241, P.O. Box 1663 Los Alamos, NM, 87545

Key Points:

- LIS and OTD data are reprocessed to correct split lightning flashes and generate gridded products including Flash Extent Density (FED)
- A global lightning climatology is generated from FED data that takes horizontal flash extent into account
- The new FED climatologies provide new perspectives on lightning frequency and human impact while confirming previous FRD findings

LA-UR-20-26320

Abstract

Previous lightning climatologies derived from Lightning Imaging Sensor (LIS) and Optical Transient Detector (OTD) total lightning measurements have quantified lightning frequency as a Flash Rate Density (FRD). This approach assumes that lightning flashes can be represented as points, and quantifies the frequency of lightning centered in each grid cell. However, lightning has a finite extent that can reach hundreds of kilometers. A new climatology based on Flash Extent Density (FED) is constructed for LIS (including ISS-LIS) and OTD that accounts for the horizontal dimension of lightning. The FED climatology documents the frequency that an observer can expect lightning to be visible overhead – regardless of where the flash began or ended.

This new FED climatology confirms and elaborates on the previous global LIS / OTD FRD and Americas-only Geostationary Lightning Mapper (GLM) findings. Applying GLM reprocessing codes to LIS and OTD data reveals cases of megaflashes measured from Low Earth Orbit that were artificially split by the LIS / OTD clustering algorithms. The FED climatology maintains Lake Maracaibo as the global lightning hotspot with an average of 389 flashes / day, but designates Karabre in the Democratic Republic of the Congo as the global thunderstorm duty (percent of the total viewtime where lightning is observed) hotspot at 7.29%. Meanwhile, Kuala Lumpur is the national capital city with the most lightning, and its airport (KUL) is the top major airport affected by lightning. The FED seasonal cycle and month-to-month changes in the "center of lightning" for the three continental chimney regions are also discussed.

Plain Language Summary

How often does lightning occur around the world? This seemingly-simple question is difficult to answer due to nuances in measuring lightning and calculating flash rates. A common methodology for answering this question is to use the concept of Flash Rate Density (FRD). This approach quantifies lightning rates by approximating lightning as points. Lightning flashes often have appreciable horizontal extents, however, that can even reach extreme sizes.

In this study we use the concept of Flash Extent Density (FED) to produce a climatology of lightning frequency that takes the horizonal scale of lightning into account. Instead of just incrementing a single gridpoint once for each flash, FED increments all gridpoint pixels that each flash touches by one. FED addresses the question of how many flashes per year an observer at a specific location can expect to see overhead. We find that despite these methodological differences from previous FRD studies, the same global hotspots are identified – with Lake Maracaibo chief among them. However, this new approach provides new insights on the previously-noted lightning trends and elaborates on how frequent lightning impacts life on Earth.

1 Introduction

Quantifying global lightning rates has been largely motivated by the desire to document global locations that are most affected by lightning (Albrecht et al., 2016) (to be abbreviated A2016) and quantify its impacts (Holle, 2016), as well as the need to understand the link between atmospheric electricity and climate (Christian et al., 2003). To the latter motivation, thunderstorms from around the world contribute to the Global Electric Circuit (GEC: see Williams and Mareev, 2013 for a review) that integrates the diurnal cycle of atmospheric electricity into a single system (Williams, 2005) that can be measured from the ground (Williams, 1992; Hutchins et al., 2014) or from space (Mach et al., 2011; Blakeslee et al., 2014; Peterson et al., 2017). The GEC allows global bulk electrically-active convective-scale processes to be quantified in one measurement that can be trended over time to monitor climate. The GEC thus provides novel insights into long-term changes in the Earth's weather that are not captured in the temperature record. Due to the ability of lightning observations to measure global "storminess," and the effects of lightning on climate, the World Meteorological Organization (WMO) and the Global Climate Observing System (GCOS) have recognized lightning as an Essential Climate Variable (ECV) (Aich et al., 2018).

Measurements of the global flash rate have improved over time, particularly following the tremendous advancements in lightning detection capabilities that have become available during the past three decades. Early estimates of the global flash rate were around 100 flashes per second (Brooks, 1925), while estimates on this order of magnitude persisted into the 1980s with lightning detected as "streaks" in the Defense Meteorological Satellite Program (DMSP) cloud imagery (Turman and Edgar, 1982; Orville and Henderson, 1986). Following this early work, NASA developed dedicated optical instruments that could detect, precisely geolocate, and

measure the development of individual lightning flashes from space. The Optical Transient Detector (OTD: Christian et al., 2003) was the first of these instruments, and flew from 1995 until 2000 aboard the MicroLab-1 satellite (later renamed to OrbView-1). OTD was an engineering prototype for the Lightning Imaging Sensor (LIS: Christian et al., 2000), which has been deployed on the Tropical Rainfall Measuring Mission (TRMM) satellite (1997-2015) and the International Space Station (2017-present) (Blakeslee et al., 2020).

These space-based optical lightning sensors detect both CG and intracloud discharges (together, termed "total lightning"), and are thus well-suited for measuring the global total flash rate and determining how lightning is distributed across the Earth. An average global flash rate of 44 flashes s^{-1} was derived from OTD data only (Christian et al., 2003), while combining OTD data with LIS data taken from the TRMM satellite yielded 46 flashes s^{-1} (Cecil et al., 2014) (to be abbreviated C2014). These values are approximately half the global average flash rates estimated previously, and vary as a function of time following fluctuations in the insolation of the tropical landmasses over the day and throughout the year.

On local scales, average flash rates are further modified by regional weather patterns and orographic effects that lead to "hotspots" in lightning activity in certain parts of the Earth. A2016 identified Lake Maracaibo as the overall global lightning hotspot from high-resolution gridded LIS observations. Warm lake waters surrounded by mountains provide ample opportunities for convergent flow to generate thunderstorms and, as a result, Lake Maracaibo sees an average of 297 thunder days per year (A2016). Other hotspots exist in Africa and Asia, some even with comparable flash rate densities to Lake Maracaibo. Previously, Christian et al. (2003) and C2014 asserted that the Congo Basin in Africa was the overall global lightning hotspot. The primary difference between these assessments of which location on Earth has the most lightning is the

grid size employed to bin the LIS / OTD data. A2016 used a high-resolution 0.1° grid, while Christian et al. (2003) and C2014 used a relatively coarse 0.5° grid. A2016 argued that using a finer grid has the advantage of bringing out localized details in the flash rate distribution that would be smoothed over a larger area in the approach used by Christian et al. (2003) and C2014.

A2016 used their high-resolution grid of LIS Flash Rate Density (FRD) to address where the Earth's lightning hotspots are located. However, there is some nuance in their results that is introduced by the chosen approach. Expressing lightning frequency as a flash rate density assumes that whole lightning flashes can be approximated as a single point with no horizontal extent. Thus, the FRD is the number of flashes centered within a grid cell divided by the total time the grid cell was observed and the grid cell area. This gives FRD a unit of flashes per year per square-kilometer. For large grid sizes (as in Christian et al., 2003 and C2014), this approximation of lightning as a point is usually valid (but not always), as most lightning does not develop laterally over distances > 50 km (Peterson et al., 2018). However, a 0.1° grid cell (~10 km x ~10 km) only encompasses approximately 4 pixels on the LIS CCD array. LIS flashes often illuminate significantly larger areas than one of these grid cells (Peterson and Liu, 2013), while the largest flashes observed from space can develop horizontally over hundreds of kilometers (Lyons et al., 2020; Peterson, 2019; Peterson et al., 2020).

FRD is actually addressing the question of how many times per year an observer at a specified location is expected to be at the center of a lightning flash. It does not count lightning flashes that start elsewhere but extend over the observer. There are other measures of flash rate that consider the lateral extent of LIS / OTD flashes. In this study we use Flash Extent Density (FED: Lojou and Cummins, 2004) to calculate global flash rates and total thunderstorm duty (the percent of the overall instrument viewtime that lightning is observed). FED is a gridded product

that increments each point once every time it falls within the footprint of a lightning flash. Furthermore, since we are mapping whole instrument pixels to our FED grid, we can construct the FED grid at an arbitrarily fine resolution while still accounting for flashes of any size. We use this FED approach to generate global climatologies for LIS and OTD. These new climatologies allow us to quantify how many flashes per year an observer at a specified location can expect to see overhead and determine whether the global hotspots reported by A2016 change after accounting for the horizontal extent of lightning.

2 Data and Methodology

2.1 LIS / OTD Lightning Detection

LIS and OTD, as well as other lightning imagers based on the NASA design, rely on the same underlying physics to detect both cloud-to-ground and intracloud lightning. These instruments measure total lightning within their Fields of View (FOVs) with high detection efficiencies by monitoring the optical radiance in a narrow band around the 777.4 nm Oxygen emission line triplet. Electrical currents in lightning discharges cause intense heating of the atmospheric constituent gases (including Oxygen) that results in them undergoing dissociation, excitation, and recombination – generating strong optical signals at these atomic lines (Christian et al., 2000). Imagers like LIS and OTD consist of high speed (usually ~500 FPS) Charge-Coupled Device (CCD) imaging arrays combined with 777.4 nm narrowband interference filters and Real Time Event Processors (RTEPSs) (Boccippio et al., 2000). Lightning is detected as transient changes in cloud illumination from the semi stable background state in any of the pixels on the CCD array. The following sections describe LIS / OTD deployments whose lightning

observations will be considered in this study.

2.1.1 OTD Deployment on the OrbView-1 Satellite

The OrbView-1 Satellite (originally MicroLab-1) was launched into Low Earth Orbit (LEO) with an altitude of 735 km and an inclination of 70° in April 1995. The altitude of the satellite resulted in the OTD 128x128 pixel imaging array covering a 1300 km swath of the Earth with a nominal spatial resolution of ~8 km at nadir (Boccippio et al., 2000). OTD collected lightning data over a nearly five-year period from 4/13/1995 until 3/23/2000.

2.1.2 LIS Deployment on the TRMM Satellite

The Tropical Rainfall Measuring Mission (TRMM) satellite was launched into LEO in November 1997 with an inclination of 35° and initial altitude of 350 km that was boosted to 403 km in August 2001 to prolong the mission (ESA, 2020). The TRMM satellite hosted a number of instruments for measuring rainfall and observing storms (Kummerow et al., 1998) including a Precipitation Radar (PR), TRMM Microwave Imager (TMI), and Visible and Infrared Scanner (VIRS). Coincident LIS measurements determined whether the observed Precipitation Features (Liu et al., 2008) were thunderstorms and provided information on their overall convective intensity (Zipser et al, 2006).

With a reduced altitude compared to OTD, the TRMM-LIS had a smaller FOV (650 km across) with a nominal pixel resolution of 4-5 km (Boccippio et al., 2002). The smaller pixel size means that TRMM-LIS resolves lightning structure with an increased level of detail compared to OTD. TRMM-LIS also had a longer on-orbit mission. The TRMM satellite lasted a total of 17

years in orbit with the orbit decaying in the last year of operation (starting in October 2014). Final observations from TRMM-LIS were obtained on 8 April 2015.

2.1.3 LIS Deployment on the International Space Station

The flight spare LIS unit for the TRMM mission was launched to the International Space Station in February of 2017 and continues to operate at the time of writing. There are currently 3 years of ISS-LIS data available, with continued data collection continuously expanding this record. The orbit of the ISS permits the ISS-LIS to resolve lightning with a comparable spatial resolution (4 km) to TRMM-LIS, but its 51.6° inclination expands LIS coverage across a broader range of latitudes (up to 55°) (Blakeslee et al., 2020).

2.2 Identifying Flashes in the LIS / OTD Data

LIS and OTD detect lightning and artifacts as "events" on the CCD imaging array. Identifying individual lightning flashes requires additional processing (filtering and clustering) to determine which flickers of light describe distinct lightning processes. Standard LIS / OTD processing defined cluster features that approximate the cloud-top illumination from individual pulses of light (termed "groups"), sequences of pulses that define distinct lightning flashes (termed "flashes"), and clusters of lightning activity that approximate thunderstorm snapshots (termed "areas"). The construction of these features for LIS and OTD is discussed at length in Mach et al. (2007).

While these LIS and OTD flash clusters have been extensively characterized over the past quarter-century of research, relatively little attention has been placed on a unique scenario that can arise during flash clustering: when two distinct flashes occur close to one another and then a new group is detected that could belong to either flash. With LIS and OTD, "first fit" solution was implemented whereby the group would be assigned to the flash that began first in

time. The second flash is left intact, resulting in a flash count of two for the storm in question.

This first fit approach can be problematic for lightning megaflashes (Lyons et al., 2020; Peterson, 2019) that tend to develop multiple branches as they propagate horizontally. It has been shown that LIS (and OTD, by extension) trigger late in the lightning discharge (Thomas et al., 2000). If early portions of the flash development are missed (when the flash is still compact), then a horizontally-propagating lightning flash could still be split into multiple flashes that contain the groups along various branches of the larger discharge, and later illumination along these branches will not reconstruct the overall flash structure. The result is an artificial reduction in flash size and increase in flash count.

GLM, meanwhile, employs a "full fit" solution to this problem. If two different candidate flashes exist for a single group, then the existing flashes are merged into a single flash feature. This approach would facilitate the identification of megaflashes – except the operational GLM processing codes enforce hard thresholds on the maximum number of groups per flash (101 groups) and the maximum flash duration (3 s) to ensure low-latency. Once a flash feature surpasses either of these thresholds, it is terminated and a new flash is constructed from any additional groups. Unfortunately, the chosen thresholds are rather low compared to even cases in the LIS / OTD record (i.e., Peterson et al., 2017b), and megaflashes are routinely split into tens or even hundreds of degraded "flashes."

To correct GLM flash splitting, Peterson (2019) developed reprocessing algorithms that identify and merge artificially-split flashes. In this study, we apply this software to the LIS / OTD data to mitigate first fit flash splitting and generate value-added data. The reprocessing software has three primary functions. First, it contains reclustering algorithms that check the

integrity of each flash cluster to ensure that it meets a full-fit implementation of the prescribed clustering algorithm. If two flashes are identified whose groups should have been clustered into the same flash, it merges the flash features and reassigns all constituent groups / events to the new reclustered flash. Thus, the reclustering codes convert the LIS / OTD data from first fit flash features to GLM-like full fit flash features. Second, the processing software produces "series" feature data that are not included in the standard LIS / OTD clustering hierarchy. Series are periods of sustained optical emission from a single lightning flash (Peterson and Rudlosky, 2019), and are useful for describing phenomena that last longer than a single 2-ms integration frame such as continuing current (Bitzer, 2016). Third, the processing software generates new Level-2 metrics that describe the cluster features and Level-3 gridded products (to be described in the next section) based on those metrics. The most important of these Level-3 products for the present study is Flash Extent Density (FED), but others include mean flash extent, mean flash duration, and thunderstorm convective probability (Peterson et al., 2020b).

LIS / OTD reclustering results are shown as histograms of split flash count per reclustered flash in Figure 1 for OTD, TRMM-LIS, and ISS-LIS, separately. Flash splitting occurred in 1.4% of our reclustered OTD flashes with a maximum of 69 split flashes merged into in a single reclustered flash. Reclustering reduced the size of the OTD sample by a total of 1.6%. Splitting was most prevalent in the TRMM-LIS data. While the maximum number of split flashes per reclustered flash was lower than OTD at 22 merged flashes, correcting this splitting reduced the sample size by 5.1%. Similarly, ISS-LIS reclustered flashes contained a maximum of 17 split flashes and correcting this led to a 4.1% reduction in sample size.

These reclustering statistics include all LIS / OTD flashes. Some flashes encounter fatal errors from the instrument, the platform, or the standard processing. Table 1 compares the total

number of reclustered flashes with the number of non-fatal flashes for each instrument. These flash counts are derived from reprocessed LIS / OTD data that have had the Detection Efficiency correction from C2014 applied. Removing the flashes with fatal quality flags reduces the OTD sample by a further 1.9% and either LIS sample by ~0.05%. While this reduction is on a similar scale to the reclustering correction for OTD, it is negligible, by comparison, for LIS.

2.3 Defining LIS / OTD Gridded (Level-3) Products

The reprocessed lightning cluster feature data with non-fatal error flags is used to generate gridded Level-3 products on a standardized grid. We elect to base our grid on a quasi-equidistant model to maintain a nearly-constant pixel size across the globe. The grid is not perfectly equidistant to increase the computational efficiency of mapping LIS / OTD pixel polygons to the output grid. Computing the positions of each corner and side of the output grid polygon would add significant computational expense. Using pixels whose corners are aligned in latitude and longitude simplifies the pixel mapping. Our grid is thus defined on a geographic grid where the southern, western, and eastern sides of a given grid cell have a specified dimension (i.e., 5 km, 10 km, etc.). The northern side of each pixel will have the same longitude range as the southern side, causing it to be longer than the southern side in the Southern Hemisphere and shorter in the Northern Hemisphere. As long as the grid size is small (tens of kilometers), the different lengths of the northern and southern grid cell boundaries will be negligible over the range of latitudes where significant lightning occurs.

However, even at larger grid sizes (hundreds of kilometers), the variations in pixel area that result from this non-uniform distance and the grid cell origin being located at its southwestern corner are still small compared to the geographic grids used in C2014 and A2016.

Figure 2 depicts the geometry of an example 150 km quasi-equidistant grid. Figure 2a shows distributions of pixel area over the latitudes with notable lightning activity (60° S to 75° N) for the 150 km grid (black, solid), a 10-km grid (black, dashed), and a geographic grid (blue). Grid sizes are normalized relative to the area of the largest cell in each grid. Figure 2b maps the boundaries of each grid cell in the 150-km grid, and also shows the swaths of example OTD (red), TRMM-LIS (purple), and ISS-LIS (blue) orbits. Dashed horizontal lines indicate the furthest extent of each instrument swath, while black + symbols denote individual flash centroids in the example orbits.

Under the geographic grids used by C2014 and A2016, the area of each grid cell decreases from the equator to the poles. The gridpoints at 60° are only half the size of the gridpoints at the equator, while pixel area decreases to 25% by 75° latitude. At the same time, the lightning frequency decreases with latitude. At higher latitudes, the lightning sample detected by OTD only (with limited temporal coverage) is divided between smaller grid cells that accentuate localized features in the distribution (for instance, individual convective-scale thunderstorms).

Grid cell sizes in quasi-equidistant grids, meanwhile, decrease from the grid origin at 85 S. For the 150 km grid shown in Figure 2b (solid line in Figure 2a), the grid maintains its nominal pixel area to within 6% over the entire electrically-active portion of the globe. For the 10-km grid (dashed line), grid cell area only differs by 0.4% over this domain. For larger 100+ km grids, cell area consistency could be improved by using the lowest latitude grid cell boundary rather than always the southern boundary to calculate grid cell geometry. However, the improvement is only marginal for the for the smaller grids that we consider in this study.

Beyond grid geometry, the other significant difference in our approach compared to the previous studies is our use of FED rather than FRD to quantify lightning frequency. Figure 3 shows how each product is generated from the original LIS point detections. FRD is based on the number of flashes detected by LIS. The locations of LIS flash centroids in an example thunderstorm are shown as + symbols in Figure 3a. These individual flashes are counted on a geographic grid, for example the 0.1° grid shown in Figure 3c, and then FRD is computed by dividing the flash count by the thunderstorm viewtime and the grid cell area.

FED is calculated from the events that comprise each group and flash. Figure 3b shows the centroid locations of LIS events for the same example thunderstorm. Note that the + symbols denoting event positions change over time following the motion of the satellite. The thunderstorm boundaries are evident from the dense cluster of events because the storm continues to flash as the satellite moves in its orbit. These events describe the lateral extent of the flashes shown as single points in Figure 1a. For each event in each flash, we map the boundaries of the illuminated pixel using geolocation codes in the LIS/OTD analysis software package and then identify each grid cell in our quasi-equidistant grid that is touched by that LIS pixel. FED is computed by incrementing each of these pixels that fall even partially within the flash footprint once per flash. The result is the grid in Figure 3d. Since we are looking only at LIS, a 5-km grid is used to match its nominal pixel size. As with FRD, FED is reported as a flash rate by dividing the FED count in Figure 3d by the thunderstorm viewtime.

We can also divide FED by grid cell area to match the FRD units of flashes per year per square kilometer. Dividing by area is certainly important for larger grids (i.e., 50 km, 100 km) to account for the broad spatial domains that are contained in a single grid cell. However, this unit does not convey the amount of lightning that an observer at a specific location would view over a

given period of time in the same way that a simple flash rate does (i.e., flashes per year). For this reason, when discussing the smaller 10-km grids, we assume that each grid cell is representative of the overhead field of view for an observer located within the cell. Thus, the fine FED grids in units of flashes per day quantify the amount of lightning that an observer can expect to see overhead.

Even with the same units, the flash counts quantified using the FRD methodology in Figure 3c differ substantially from those quantified using the FED methodology in Figure 3d. In Figure 3c, lightning activity is limited to the convective core of the thunderstorm, and a maximum of 7 flashes were detected at any given location. Taking the horizontal extent of each LIS flash into account causes the flash counts in Figure 3d to be greater (peaking at 16) and lightning activity to be counted over the full thunderstorm area. The flash rate is considered zero for an observer at 35.1° E, 28.4° S in Figure 3c (despite being nearly surrounded by flashing pixels), but the observer would have detected ~10 flashes in Figure 3d using the FED approach.

The numerical difference between FRD and FED is a strong function of grid geometry, which includes both its resolution and manner of construction. To focus on the resolution effect, we compare the average FED and FRD values from a sample of 1000 LIS orbits in Figure 4 that result from identical quasi-equidistant grids whose resolutions range from 5 km to 250 km. For the smallest 5-km grid, the average FRD in locations with lightning was only 3% of the average FED. This mostly comes from pixels where FED > 0 while FRD = 0. For a 10-km grid (comparable to the 0.1° grid in A2016, the FRD is still only 9% of the FED, on average. We can expect 11x more lightning to occur over a given location than what is reported by FRD. By 50 km (similar to the 0.5° grid used by C2014), FRD is 40% of the FED. Finally, by 250 km (similar to the 2.5° grid in C2014), the FRD is 80% of the FED. Note that the fraction does not

reach unity by these coarse grid sizes. Since FED accounts for lateral flash extent, there is always the possibility that lightning near the edge of a grid cell will cause the FED to extend into the neighboring cell. This becomes less common as the grid spacing increases, but it does not disappear completely over the scales shown in Figure 4.

We use these quasi-equidistant grids to produce the full suite of gridded products that we generate for GLM for LIS and OTD in our reclustered dataset. These Level-3 products provide contextual information about the other flashes that occur in the vicinity of an observed flash and the convective state of the parent thunderstorm. This information is particularly important for validating OTD and ISS-LIS flashes, since these platforms lack coincident meteorological observations.

For example, Figure 5 shows cases of OTD and LIS megaflashes that exceed 100 km in extent. To date, no cases of valid megaflashes have been reported from an instrument in LEO. The largest LIS and OTD flashes in the original science dataset were instrument artifacts rather than natural lightning observations (Peterson et al., 2017). The cases in Figure 5 are reclustered flashes with the OTD case (Figure 5a) containing 5 merged flashes and the LIS case (Figure 5b) containing 14 merged flashes. The time-ordered group extent by longitude (top) and group extent by latitude (right) plots next to the map show the consistent and logical trajectory over time that occurs in valid GLM megaflashes. The map shows the group-level structure (line segments) and a convex hull around the events (solid contour) on top of the FED for each gridpoint (in flashes per minute). Both flashes start in convective features with high FED values and then propagate northward (OTD) or westward (LIS) into regions of low FED values consistent with an electrified stratiform region. The ordered progression of the groups and the meteorological context for the apparent development of the flash fit with our understanding of megaflashes.

Thus, there were a small number of megaflashes mapped by OTD and LIS (compared to GLM) despite their limited viewtime over favorable thunderstorms for megaflash activity. These flashes were just split by the first-fit clustering, and that is why they were not identified in the original LIS / OTD science datasets.

2.4 Integrating LIS / OTD FED Grids into a Global Climatology

We reprocess each LIS and OTD orbit file from the original science data and compute all Level-3 products on both a 10 km grid and a 50 km grid. These grids are standardized between orbits, permitting their direct summation. An FED climatology is constructed by accumulating the OTD, TRMM-LIS, and ISS-LIS grids over time. The LIS / OTD FED annua, seasonal, and monthly climatologies are hosted at Peterson (2020). This study will discuss the annual-averaged climatology (LRFC / HRFC in C2014, VHRFC in A2016) and the three-month seasonal FED climatology. Smoothing is not applied for two reasons. First, as A2016 notes, smoothing dilutes localized features such as orographic enhancement. Second, the FED approach and the quasi-equidistant grid improve spatial data filling, while ISS-LIS adds additional observations to the mid-latitudes that were not available to C2014. The amount and type of data that we consider are sufficient to produce an annual-averaged climatology at a fine resolution without smoothing.

However, partitioning the data into temporal bins reduces the coverage at high latitudes past the point where a fine 10-km resolution is feasible. The reason for this is illustrated in the global distribution of total viewtime from all three instruments in Figure 6. Viewtime is mapped in Figure 6b with political boundaries (thin lines) and continental boundaries (thick lines) overlaid. Oceanic grid cells are assigned to the nearest continent. Average (purple) and maximum (blue) viewtimes for each latitude (Figure 6a) or longitude (Figure 6b) slice are shown

to the left and below the map. While grid cells within the observation domain of all three instruments have accumulated an average of 200 to 600 hours of viewtime, locations that were observed by only OTD / ISS-LIS or only OTD, have only 100 – 200 hours of observations available. Even dividing this sample into four seasonal bins causes local maxima from individual active storms outside of the TRMM-LIS domain to become prominent features in certain locations on the 10-km grid. We mitigate this issue by examining the seasonal distributions on a relatively-coarse 50-km grid.

As in A2016 we employ reverse geocoding to identify the nearest named places to the lightning FED hotspots. This is accomplished with the same GeoNames geographical database (Wick, 2006) that was used by A2016. We use the 10-km grids to generate lists of the top 10 hotspot locations on each continent and their nearest associated place names. A2016 employed a 100 km restriction on hotspot selection. If a gridpoint had sufficiently-high FRD values to be identified as a hotspot, but occurred within 100 km of another hotspot, then it was not considered distinct and not listed. This approach prevents all of the gridpoints over Lake Maracaibo, for example, from dominating the list of global hotspots. We use the 100-km separation from A2016 in our analyses of FED hotspots. Though this distance-based definition of hotspot clusters is arbitrary, and new methods exists that formalize the construction of lightning FRD hotspot clusters (de Abreu et al., 2020), the global scope of the lists in A2016 will facilitate comparisons between the FRD and FED distributions.

Once hotspot pixels are identified, A2016 imposed an additional restriction on what place names are reported: the reported place must have a population of at least 1000 inhabitants. While it may be beneficial to report potentially recognizable place names to a general audience in the lightning hotspot lists, doing so introduces a bias towards population centers. Some of the named

locations are tens or even hundreds of kilometers from the hotspot gridpoint. To mitigate some of this bias, we do not enforce a population threshold on the reported place names. This bias will still exist, however, as the GeoNames database is far from complete. Particularly in remote locations, named places exist that are not listed in the database. Furthermore, oceanic hotspot gridpoints will always be associated with whichever land-based location happens to be closest. However, this only affects the names of the nearest place, not the pixel location. Thus, it does not prevent direct comparisons with A2016.

3 Results

3.1 Global LIS / OTD FED Lightning Climatology

3.1.1 Annual Average Flash Rate

The global annual average flash rate distribution derived from FED data rather than FRD data is presented in Figure 7 on a 10-km grid. This global distribution describes how much lightning an observer at each point on the map can expect to experience, on average. In addition to the global map (Figure 7b), average (purple) and maximum (blue) flash rates by latitude (Figure 7a) and longitude (Figure 7c) are shown to the left of and below the map. As in Figure 6, the global LIS / OTD domain is divided between the continents of North America, South America, Europe, Africa, Asia, and Oceania with oceanic grid cells assigned to the nearest continent. Then, for each continent, the top 10 FED hotspots are indicated with X symbols. Full-resolution images of longitude quadrants that are aligned to continental boundaries are also shown as Supplemental Information in S1 to S4 that preserve some of the fine details that are not readily apparent in Figure 7.

While FED and FRD may differ numerically, the global distribution of lightning activity captured in the FED climatology is nearly identical to previous FRD climatologies from Boccippio et al. (2000), Christian et al., (2003), C2014, and A2016. Frequent lightning activity is driven by the insolation of the Earth's landmasses and circulation patterns that result from orographic effects or land / sea interactions. Thus, lightning is most frequent in the tropics (Figure 7a) where insolation is greatest throughout the year, and is concentrated into the three longitudinal "chimney" regions (Figure 7c) that are defined by the continents of North America / South America, Europe / Africa, and Asia / Oceania. These chimneys each account for roughly 90 degrees longitude in Figure 7c. The South Pacific Convergence Zone (SPCZ) is typically considered a fourth chimney that captures the remaining ~90 degrees longitude in discussions of the GEC. Our continental mask, however, divides the SPCZ between the continents of Oceania and South America.

Lightning FED hotspots occur in tropical regions with complex terrain where mountains or coastlines provide enhanced opportunities for convergence to lead to thunderstorm activity. In North America, the hotspots are spread across coastal Central America and the larger islands in the Gulf of Mexico and the Caribbean Sea. In South America, hotspots are located over Lake Maracaibo, in the coastal mountains of Colombia, and in the inland Andes further south. In Europe, hotspots occur throughout the coastal Mediterranean Sea (both onshore and offshore), and in Northern Italy at the base of the Alps. In Africa, hotspots are located in the Congo Basin – particularly along the mountain ranges in the Democratic Republic of the Congo – or at the delta of the Akpa Yafe River between Nigeria and Cameroon. In Asia, the hotspots are located along the foothills of the Himalayas in Pakistan and Northern India, in Meghalaya near the India / Bangladesh border, and in the coastal mountains of Indonesia and Malaysia and the Strait of

Malacca between them. Finally, the hotspots in Oceania are divided between the northern Australian coast and the complex terrain of Papua New Guinea. These broad geographic regions are consistent with hotspot clusters in A2016.

The top 10 FED hotspots from each continent are listed in Table 2 along with the nearest named place. Lake Maracaibo is the overall top global FED hotspot with an average of 389 flashes per day over the hotspot grid cell (9.62 N, 71.8 W). The nearest place is San Carlos del Zulia in Venezuela, which is 70 km from the hotspot grid cell over the lake. A2016 likewise named Lake Maracaibo as the overall top FRD hotspot. Due to differences in FED and FRD, and in grid geometry, the location of their top grid cell (9.75 N, 71.65 W) is 22 km away from the top FED hotspot with a different named place (Lagunillas, Venezuela) yielded by reverse geolocation. The second (369 flashes / day), third (315 flashes / day), and fourth (314 flashes / day) top global FED hotspots are located in the Kivu region within the Congo Basin in Africa. The nearest places to each of these hotspots (Karabe and Sake) are >100 km away in each case.

The top ranked hotspot that is not in South America or Africa is Rio Bravo, Guatemala (rank 11). This top hotspot for North America sees an average of 217 flashes per day. The remaining top continental hotspots are Subang Jaya, Malaysia for Asia (rank 16 with 198 flashes / day), Derby, Australia for Oceania (rank 170 with 120 flashes / day), and Pognana Lario, Italy (rank 564 with 82 flashes / day). Of the five continents considered in both A2016 and this study, four of the top hotspots matched to within 25 km between the FED and FRD methodologies. While there were locations in the hotspot rankings below the top spot in A2016 that do not appear in our Table 2 (for example, Mount Lisa, Australia at FRD rank 9 for Oceania), most of the hotspot regions appear in both lists. However, they are re-ordered due to the methodical differences. This is also why the top Asia hotspot differs between the two studies. Daggar,

Pakistan was identified as the top FRD hotspot for Asia in A2016. It is ranked in second place in terms of FED in Table 2 behind Subang Jaya, Malaysia. The difference in FED between these two hotspots is only 16 flashes per day, resulting in global rankings of 16 and 22, respectively.

3.1.2 Annual Average Thunderstorm Duty

In addition to quantifying flash rates that describe how much lightning extends overhead in each global grid cell, our Level-3 gridded data based on the FED concept can be used to calculate thunderstorm duty (Peterson, 2019), which is a measure of thunderstorm frequency rather than lightning frequency. The concept of thunderstorm duty is similar to that of thunder days that counts the number of unique calendar days where thunder is detected. However, a single isolated lighting flash counts the same in terms of thunder days as a long-lived thunderstorm that persists over a location for many hours. For this reason, the number of thunder days is not an ideal measure of thunderstorm impact.

Thunderstorm duty mitigates this issue by measuring the amount of time that a thunderstorm is observed compared to the total amount of time sampled. We define thunderstorm duty as the percentage of the LIS / OTD viewtime for each gridpoint (Figure 6) where lightning is observed. This formulation of thunderstorm duty is based on Peterson (2019), which used continuous GLM measurements. The low Earth orbits of LIS and OTD limit their measurements to minute-scale snapshots of each thunderstorm. We add the reported viewtime to the duty for a given gridpoint if at least one lightning event occurs at that location. Otherwise, no duty is added. Due to the limited viewtime per orbit, the thunderstorm duty from our approach will be similar to the LIS thunderstorm occurrence climatologies presented in Cecil et al. (2015), where thunderstorm occurrence was quantified by dividing the number of orbits where lightning was observed in each 0.5 degree grid cell by the number of orbits where that grid cell was observed.

Notable variations between these climatologies and thunderstorm duty will be largely driven by differences in grid geometry and the use of FED rather than FRD to quantify thunderstorm frequency.

The annual-average global LIS / OTD thunderstorm duty distribution is presented in Figure 8 in the same manner as the FED distribution in Figure 7 or the viewtime distribution in Figure 6. As with Figure 7, we also show detailed images of longitude quadrants that bound the continents in S5-S8. Thunderstorm duty around the world peaks at 3-7% of the total viewtime. These percentages are consistent with the GLM results in Peterson (2019), which reported an equivalent of 10-20 days of total accumulated thunderstorm duty in the tropical Americas over a year-long period. This corresponds to between 2.7% - 5.5% of the GLM viewtime.

Thunderstorm duty is far more sensitive to low total viewtimes than the previous FED flash rate analysis. The minimum duty value that can be reported depends on the total viewtime for a given grid cell. For low flash rate gridpoints that were only infrequently sampled by ISS-LIS and / or OTD, the all-viewtime-or-nothing duty definition leads to sparse coverage outside of the TRMM-LIS domain and sharp lines in Figure 8 along the outer latitudes for this domain. The maximum viewtimes of between 200 and 600 hours (8-25 days) can still be insufficient to resolve fine structure in the thunderstorm duty distribution – for example, reductions in duty of the Amazon river system noted in Peterson (2019). GLM has a clear advantage in measuring thunderstorm duty because its continuous sampling adds 365 days of viewtime per year over its entire hemispheric-scale FOV. However, it still lacks the global coverage and decade-long record of LIS / OTD.

Global thunderstorm duty hotspots on each continent are depicted as X symbols in Figure 8 and listed in Table 3. While many of the entries are near (if not the same as) the FED flash rate

hotspots in Table 2, certain regions have greater thunderstorm duties than indicated by their FED frequencies. For example, the named places in Cuba, Bolivia, India, and Australia that rank among the continental hotspots in Table 2 are missing in Table 3. All duty hotspots in the Congo Basin in Africa are additionally located in the Kivu region (and surrounding regions) and not areas further west, while Malaysia and Indonesia account for all of the hotspots in Asia.

3.1.3 LIS / OTD FED Lightning Climatology Applications

The FED-based flash rate and thunderstorm duty distributions can be used to quantify lightning hazards and impacts on daily life. As two examples, we identify and rank the top national capital cities and the top major airports for lightning activity. Capital city locations are determined from geolocation data, while the airport locations and ancillary data are derived from Megginson (2007). Table 4 shows the top-ranked capital cities by either FED flash rate or by thunderstorm duty. The top spot on both lists is Kuala Lumpur, Malaysia, which has an average of 179 flashes per day and a 4.21% thunderstorm duty. The FED list then continues with Islamabad, Pakistan (158 fl/day, 2.13% duty), Singapore (138 fl/day, 3.39% duty), Havana, Cuba (127 fl/day, 1.99% duty), and Panama City (106 fl/day, 2.66% duty). These cities appear on both lists and thus have high flash rates spread across relatively long periods of time – increasing the overall impact of lightning compared to the other capital cities.

We perform the same exercise with major airports in Table 5. While Jose Marti International Airport (HAV) in Havana, Cuba has the most lightning, Kuala Lumpur International Airport (KUL) in Kuala Lumpur, Malaysia is most affected by lightning, overall, as it takes the top spot for thunderstorm duty as well as the second spot for FED flash rate. Singapore Changi (SIN) similarly ranks highly in both lists – indicating an exceptional quantity of lightning and a relatively large duty that might hamper operations. One airport in the United

States ranks among the global major airports most impacted by lightning in the world: Southwest Florida International Airport (RSW) in Fort Myers has an average of 105 fl/day and a thunderstorm duty of 2.03%.

3.2 Global LIS / OTD FED Seasonal Lightning Climatology

The global lightning distributions shown in Section 3.1 are averaged over the entire year. The frequency of lightning and locations where it is particularly common vary from month to month following changes in insolation and local atmospheric forcing. In this section, we examine the seasonal cycle in the global FED distribution. Rather than focus on hotspots, as in Section 3.1, we examine continental-scale changes in the three primary chimney regions: North and South America, Europe and Africa, and Asia and Oceania. For each continental chimney, we compute the "center of lightning" (calculated similarly to center of mass where FED is used for the weighting) for each month of the year and then track how it moves over time.

3.2.1 December – February

The global FED distribution for December – February is shown in Figure 9 in the style of Figure 7. To avoid the sampling issues in the cold season hemisphere and at higher latitudes, we use the 50 km gridded climatology rather than the 10 km grid shown previously. Because 50 km is large enough that a single pixel may no longer be a reasonable approximation for what an observer would see overhead, we divide the FED flash rate by the grid cell area as in C2014 and A2016. The annual cycle is also animated in S9 with monthly versions of the plot shown in Figure 9.

During the northern hemisphere winter, the Americas center of lightning is located on the Brazil / Bolivia border, the Europe and Africa center of lightning is located on the Democratic

Republic of the Congo / Angola border, and the Asia and Oceania center of lightning is located near Darwin, Australia. The specific locations of the centers of lightning vary between the individual months, and are furthest south in January. The little lightning that occurs in the northern hemisphere outside of the inner tropics is concentrated over the southern United States and neighboring offshore regions in the Gulf of Mexico and Gulf Stream, over the Mediterranean Sea off the coast of Anatolia, over the Red Sea and Persian Gulf, and in northern India and Pakistan. Only sporadic lightning activity is noted in the northern interiors of the North American, European, and Asian continents.

3.2.2 March – May

March through May marks the transition of lightning activity from the Southern Hemisphere to the Northern Hemisphere. Flashes are noted up to high northern latitudes in Figure 10 while the FED maxima are concentrated in the tropical belt. As a result, the centers of lightning straddle the equator from March to May with a greater northern displacement in the Americas and Asia due to a combination of hemispheric differences in landmass and a northern hemisphere bias in hotspot locations with particularly favorable terrain for frequent lightning (Colombia and Lake Maracaibo at 5-10 N, and eastern India and Bangladesh at 20-25N). This northern offset is not noted for the Europe and Africa chimney where the primary Kivu hotspot in the Congo Basin in Africa is located near the equator.

3.2.3 June – August

The center of lightning for each chimney reaches its furthest northern position during the Northern Hemisphere summer between June and August (Figure 11). In the Americas, the northern extreme for the center of lightning is located near the northern coast of Cuba in July. In Africa and Europe, the center of lightning is located in Chad during all three months. Finally, in

Asia and Oceania, the northernmost center of lightning reaches Tibet also in July. These northern locations for the centers of lightning are helped by lightning activity extending throughout the northern hemisphere continents – up to their northern shores on the Arctic Ocean. The relatively infrequent lightning that occurs in the Southern Hemisphere is concentrated along the east coasts of the southern landmasses – southeastern Brazil, Uruguay, Argentina, and Paraguay and adjacent offshore regions, and the coastal waters off the eastern coasts of South Africa and Australia.

3.2.4 September - November

The final season – September to November – marks the transition from the northern hemisphere maximum in insolation to a southern hemisphere maximum. FED values in Figure 12 retreat from the northern high latitudes as intense thunderstorms in places like the La Plata basin in South America and the northern coast of Australia bring greater FED values to the Southern Hemisphere than in the spring. As a result, the centers of lightning in the Americas and Asia and Oceania are further south in November than they were in March. The lightning in Europe and Africa does not migrate southward as quickly as the other two continental chimneys, causing the November center of lightning to be slightly to the north of its March position.

The circuits that the centers of lightning take over the year through the Americas and Europe and Africa are essentially identical from January to July and July to January. Despite shifts in latitude position during like months, the longitude positions are close enough that the circuits can be approximated as lines. However, in Asia and Oceania, the winter-to-summer route to the northernmost center of lightning extends further west than the summer-to-winter route to its southernmost location. The circuit essentially encircles western Laos and northern Thailand after diverging off the coast of Sarawak, Malaysia. South of this point, the northern and southern

602 paths of the Asia and Oceania center of lightning converge like the other two chimneys. This
603 difference between the winter-to-summer and summer-to-winter circuits is due to widespread
604 lightning activity in western and central Asia and concentrated hotspots in India and Bangladesh
605 in the northern hemisphere spring that are not observed in the fall.
606

607 **4 Conclusion**

608 This study constructs a LIS / OTD lightning climatology based on FED rather than FRD
609 data, which accounts for the horizontal extent of lightning flashes. Employing an FED approach
610 increases the overall flash rates reported by OTD, TRMM-LIS, and ISS-LIS by counting flashes
611 that originated elsewhere before developing horizontally over each gridpoint. However, the
612 normalized global lightning distribution remains largely unchanged from the previous FRD
613 assessments. Many of the global FRD hotspots – including the top hotspot of Lake Maracaibo
614 (389 flashes / day) – are also the top hotspots in terms of FED.
615 The FED approach is also used to calculate thunderstorm duty across the globe.
616 Thunderstorm duty is defined as the percent of the overall instrument viewtime when lightning is
617 observed. Top locations for thunderstorm duty reach 3-7% - in line with recent GLM duty
618 measurements over the Americas. The overall top hotspot for thunderstorm is Kabare,
619 Democratic Republic of the Congo at 6.68%.
620 The fine resolution (10 km) FED climatology may be used to quantify lightning impacts
621 on daily life. Many of the global lightning hotspots occur in remote areas far from inhabited
622 places. The fine resolution grids can be used to rank types of places according to potential
623 lightning impact. For example, we determine that Kuala Lumpur, Malaysia is the national capital
624 city with both the most lightning (179 flashes / day) and the greatest thunderstorm duty (4.21%).

Its airport (KUL) also happens to be the global major airport most affected by lightning. Other potential analyses that could be undertaken include ranking major global population centers or sporting venues, or finding the lightning hotspots in each country or state.

In addition to the annual average global climatology, we also produce a seasonal FED climatology on a 50 km grid and track the migration of lightning from the Southern Hemisphere in January to the Northern Hemisphere in July. A "center of lightning" method (based on the definition of center of mass) is used to track continental-scale changes in the lightning distribution in each of the three primary chimneys: the Americas, Europe and Africa, and Asia and Oceania. Differences in landmass north or south of the equator as well as a northern offset for two of the three lightning hotspots result in a northern bias in the centers of lightning in all three chimneys. While the centers of lightning over the Americas and Europe and Africa follow nearly the same linear trajectory from January to July and July to January, the centers of lightning for Asia and Oceanic follow a circuit around Thailand and Laos due to the lightning centers in the northern hemisphere spring being located further west than the lightning centers in the northern hemisphere fall.

These results illustrate a small sample of the diverse collection of applications that are enabled by this type of dataset. This data is particularly useful for documenting societal impacts from the total lightning (CG plus IC) that space-based instruments like LIS and OTD can sense. The level of detail in these global maps (and the overall value of the analyses that they enable) will continue to improve as long as LIS remains operational on the International Space Station. Geostationary platforms like GLM – while providing a tremendous volume of data – individually lack the global coverage necessary for such analyses. However, data fusion between geostationary systems including GLM, LMI, and the future LI (Goodman et al., 2013; Yang et

al., 2017; Kokou et al., 2018) may eventually provide nearly-global continuous lightning coverage to facilitate such analyses.

This future capability highlights the need for standardization in the clustering algorithms employed by the various space-based lightning sensors. The reclustering results shown here demonstrate that FRD and FED values (and other Level-3 gridded products) are sensitive to what each instrument considers a "flash." A standardized sensor-agnostic lightning feature dataset that combines the best practices demonstrated by each instrument would ensure that a "flash" seen by one instrument is completely compatible with the flashes seen by the other instruments – whether it is a small convective-scale discharge or a horizontally-extensive megaflash. Future work will further investigate this concept.

Acknowledgments

This work was supported by the US Department of Energy through the Los Alamos National Laboratory (LANL) Laboratory Directed Research and Development (LDRD) program under project number 20200529ECR. Los Alamos National Laboratory is operated by Triad National Security, LLC, for the National Nuclear Security Administration of U.S. Department of Energy (Contract No. 89233218CNA000001). The work by co-author Douglas Mach was also supported by NASA 80MFSC17M0022 "Cooperative Agreement with Universities Space Research Association" and NASA Research Opportunities in Space and Earth Science grant NNX17AJ10G "U.S. and European Geostationary Lightning Sensor Cross-Validation Study." The work by co-author Dennis Buechler of the University of Alabama in Huntsville (UAH) was conducted under Cooperative Agreement NNM11AA01A (*Lightning Imaging Sensor on International Space Station*) with the NASA MSFC. The LIS (Blakeslee, 1998; Blakeslee, 2019)

and OTD (Blakeslee et al., 1996) data sets may be accessed via the NASA Global Hydrology Resource Center DAAC via the DOIs listed below. The LIS / OTD FED annual, seasonal, and monthly climatologies are hosted at Peterson (2020). The GeoNames database (Wick, 2005) used in this study may be accessed via http://www.geonames.org. The OurAirports data (Megginson, 2007) used in this study may be accessed via https://ourairports.com/data/.

References

de Abreu, L. P., Gonçalves, W. A., Mattos, E. V., & Albrecht, R. I. (2020). Assessment of the total lightning flash rate density (FRD) in northeast Brazil (NEB) based on TRMM orbital data from 1998 to 2013. *International Journal of Applied Earth Observation and Geoinformation*, *93*, 102195.

Aich, V., Holzworth, R., Goodman, S., Kuleshov, Y., Price, C., & Williams, E. (2018). Lightning: A new essential climate variable. *Eos*, **99**. https://eos.org/science-updates/lightning-a-new-essential-climate-variable

Albrecht, R. I., S. J. Goodman, D. E. Buechler, R. J. Blakeslee, and H. J. Christian, 2016: Where Are the Lightning Hotspots on Earth?. *Bull. Amer. Meteor. Soc.*, **97**, 2051–2068, https://doi.org/10.1175/BAMS-D-14-00193.1.

Blakeslee, Richard J.. 1996. *OPTICAL TRANSIENT DETECTOR (OTD) LIGHTNING* [Science Data]. Dataset available online from the NASA Global Hydrology Resource Center DAAC, Huntsville, Alabama, U.S.A. DOI: http://dx.doi.org/10.5067/LIS/OTD/DATA101

Blakeslee, Richard J.. 1998. *Lightning Imaging Sensor (LIS) on TRMM Science Data* [Science Data]. Dataset available online from the NASA Global Hydrology Resource Center DAAC, Huntsville, Alabama, U.S.A. DOI: http://dx.doi.org/10.5067/LIS/LIS/DATA201.

Blakeslee, Richard J.. 2019. *Non-Quality Controlled Lightning Imaging Sensor (LIS) on International Space Station (ISS) Science Data* [NQC Science Data]. Dataset available online from the NASA Global Hydrology Resource Center DAAC, Huntsville, Alabama, U.S.A. DOI: http://dx.doi.org/10.5067/LIS/ISSLIS/DATA107

Blakeslee, R. J., Mach, D. M., Bateman, M. G., & Bailey, J. C. (2014). Seasonal variations in the lightning diurnal cycle and implications for the global electric circuit. *Atmospheric research*, *135*, 228-243. https://doi.org/10.1016/j.atmosres.2012.09.023

Blakeslee, R. J., T. J. Lang, W. J. Koshak, D. Buechler, P. Gatlin, D. M. Mach, G. T. Stano, K. S. Virts, T. D. Walker, D. J. Cecil, W. Ellett, S. J. Goodman, S. Harrison, D. L. Hawkins, M. Heumesser, H. Lin, M. Maskey, C. J. Schultz, M. Stewart, M. Bateman, O. Chanrion, and H. Christian (2020). Three years of the Lightning Imaging Sensor on board the International Space Station: Expanded global coverage and enhanced applications.

Journal of Geophysical Research: Atmospheres, **125**, e2020JD032918. https://doi.org/10.1029/2020JD032918

Bitzer, P. M. (2017), Global distribution and properties of continuing current in lightning, *J. Geophys. Res. Atmos.*, 122, 1033– 1041, doi:10.1002/2016JD025532.

Boccippio, D. J., and Coauthors, 2000: The Optical Transient Detector (OTD): Instrument Characteristics and Cross-Sensor Validation. *J. Atmos. Oceanic Technol.*, **17**, 441–458, https://doi.org/10.1175/1520-0426(2000)017<0441:TOTDOI>2.0.CO;2.

Boccippio, D. J., W. J. Koshak, and R. J. Blakeslee, 2002: Performance Assessment of the Optical Transient Detector and Lightning Imaging Sensor. Part I: Predicted Diurnal Variability. *J. Atmos. Oceanic Technol.*, **19**, 1318–1332, https://doi.org/10.1175/1520-0426(2002)019<1318:PAOTOT>2.0.CO;2.

Brooks, C. E. P., The distribution of thunderstorms over the globe, Geophys. Memo., 3(24), 147–164, 1925.

Cecil, D. J., Buechler, D. E., & Blakeslee, R. J. (2014). Gridded lightning climatology from TRMM-LIS and OTD: Dataset description. *Atmospheric Research, 135*, 404-414. https://doi.org/10.1016/j.atmosres.2012.06.028

Cecil, D. J., D. E. Buechler, and R. J. Blakeslee (2015). TRMM LIS Climatology of Thunderstorm Occurrence and Conditional Lightning Flash Rates. *J. Climate*, **28**, 6536–6547, https://doi.org/10.1175/JCLI-D-15-0124.1.

Christian, H. J., R. J. Blakeslee, S. J. Goodman, and D. M. Mach (Eds.), 2000: Algorithm Theoretical Basis Document (ATBD) for the Lightning Imaging Sensor (LIS), NASA/Marshall Space Flight Center, Alabama. (Available as http://eospso.gsfc.nasa.gov/atbd/listables.html, posted 1 Feb. 2000)

Christian, H. J., et al., Global frequency and distribution of lightning as observed from space by the Optical Transient Detector, *J. Geophys. Res.*, 108(D1), 4005, doi:10.1029/2002JD002347, 2003.

ESA, 2020: TRMM (Tropical Rainfall Measuring Mission). Accessed 7/11/2020. https://directory.eoportal.org/web/eoportal/satellite-missions/t/trmm

Holle, R. L., 2016: A Summary of Recent National-Scale Lightning Fatality Studies. *Wea. Climate Soc.*, **8**, 35–42, https://doi.org/10.1175/WCAS-D-15-0032.1.

Hutchins, M. L., Holzworth, R. H., and Brundell, J. B. (2014), Diurnal variation of the global electric circuit from clustered thunderstorms, *J. Geophys. Res. Space Physics*, 119, 620–629, doi:10.1002/2013JA019593.

Kokou, P., P. Willemsen, M. Lekouara, M. Arioua, A. Mora, P. Braembussche, E. Neri, & D. Aminou. (2018). Algorithmic chain for lightning detection and false event filtering based on the MTG lightning imager. *IEEE Transactions on Geoscience and Remote Sensing*. https://doi.org/10.1109/TGRS.2018.2808965

Kummerow, C., W. Barnes, T. Kozu, J. Shiue, and J. Simpson, 1998: The Tropical Rainfall Measuring Mission (TRMM) Sensor Package. *J. Atmos. Oceanic Technol.*, **15**, 809–817, https://doi.org/10.1175/1520-0426(1998)015<0809:TTRMMT>2.0.CO;2.

Lojou, J.-Y., & Cummins, K. L. (2004). On the representation of two- and three-dimensional total lightning information. In Preprints, Conference on Meteorological Applications of Lightning Data, Paper 2.4, AMS Annual Meeting , San Diego, CA, USA.

Liu, C., E. J. Zipser, D. J. Cecil, S. W. Nesbitt, and S. Sherwood, 2008: A Cloud and Precipitation Feature Database from Nine Years of TRMM Observations. *J. Appl. Meteor. Climatol.*, **47**, 2712–2728, https://doi.org/10.1175/2008JAMC1890.1.

Lyons, W. A., E. C. Bruning, T. A. Warner, D. R. MacGorman, S. Edgington, C. Tillier, and J. Mlynarczyk, 2020: Megaflashes: Just How Long Can a Lightning Discharge Get?. *Bull. Amer. Meteor. Soc.*, **101**, E73–E86, https://doi.org/10.1175/BAMS-D-19-0033.1.

Mach, D. M., Christian, H. J., Blakeslee, R. J., Boccippio, D. J., Goodman, S. J., and Boeck, W. L. (2007), Performance assessment of the Optical Transient Detector and Lightning Imaging Sensor, *J. Geophys. Res.*, 112, D09210, doi:10.1029/2006JD007787.

Mach, D. M., Blakeslee, R. J., and Bateman, M. G. (2011), Global electric circuit implications of combined aircraft storm electric current measurements and satellite-based diurnal lightning statistics, *J. Geophys. Res.*, 116, D05201, doi:10.1029/2010JD014462.

Megginson, D. (2007). *Open data downloads*. OurAirports. https://ourairports.com/data/

Orville, R. E., and R. W. Henderson, 1986: Global Distribution of Midnight Lightning: September 1977 to August 1978. *Mon. Wea. Rev.*, **114**, 2640–2653, https://doi.org/10.1175/1520-0493(1986)114<2640:GDOMLS>2.0.CO;2.

Peterson, M., & Rudlosky, S. (2019). The time evolution of optical lightning flashes. Journal of Geophysical Research: Atmospheres, 124, 333– 349. https://doi.org/10.1029/2018JD028741

Peterson, M., and Liu, C. (2013), Characteristics of lightning flashes with exceptional illuminated areas, durations, and optical powers and surrounding storm properties in the tropics and inner subtropics, *J. Geophys. Res. Atmos.*, 118, 11,727– 11,740, doi:10.1002/jgrd.50715.

Peterson, M., Deierling, W., Liu, C., Mach, D., and Kalb, C. (2017), A TRMM/GPM retrieval of the total mean generator current for the global electric circuit, *J. Geophys. Res. Atmos.*, 122, 10,025– 10,049, doi:10.1002/2016JD026336.

Peterson, M., Rudlosky, S., & Deierling, W. (2017b). The evolution and structure of extreme optical lightning flashes. *Journal of Geophysical Research: Atmospheres*, 122, 13,370–13,386. https://doi.org/10.1002/2017JD026855

Peterson, M., Rudlosky, S., & Deierling, W. (2018). Mapping the lateral development of lightning flashes from orbit. *Journal of Geophysical Research: Atmospheres*, 123, 9674–9687. https://doi.org/10.1029/2018JD028583

Peterson, M. (2019). Research applications for the Geostationary Lightning Mapper operational lightning flash data product. *Journal of Geophysical Research: Atmospheres*, 124, 10205– 10231. https://doi.org/10.1029/2019JD031054

Peterson, M. J., Lang, T. J., Bruning, E. C., Albrecht, R., Blakeslee, R. J., Lyons, W. A., et al.. (2020). New WMO Certified Megaflash Lightning Extremes for Flash Distance (709 km) and Duration (16.73 seconds) recorded from Space. *Geophysical Research Letters*, 47, e2020GL088888. https://doi.org/10.1029/2020GL088888

Peterson, M., S. Rudlosky, and D. Zhang, 2020b: Thunderstorm Cloud-Type Classification from Space-Based Lightning Imagers. *Mon. Wea. Rev.*, **148**, 1891–1898, https://doi.org/10.1175/MWR-D-19-0365.1.

Peterson, Michael, 2020, "LIS / OTD Global Flash Extent Density (FED) Climatology", https://doi.org/10.7910/DVN/TADRNA, Harvard Dataverse, V1

Thomas, R. J., Krehbiel, P. R., Rison, W., Hamlin, T., Boccippio, D. J., Goodman, S. J., & Christian, H. J. (2000). Comparison of ground-based 3-dimensional lightning mapping observations with satellite-based LIS observations in Oklahoma. *Geophysical research letters*, *27*(12), 1703-1706.

Turman, B. N., and Edgar, B. C. (1982), Global lightning distributions at dawn and dusk, *J. Geophys. Res.*, 87(C2), 1191– 1206, doi:10.1029/JC087iC02p01191.

Wick, M. (2005). GeoNames. Retrieved August 06, 2020, from http://www.geonames.org/

Williams, E. R., The Schumann Resonance: A global tropical thermometer, Science, 256, 1184–1187, 22 May 1992 .

Williams, E. R. (2005). Lightning and climate: A review. *Atmospheric research*, *76*(1-4), 272-287.

Williams, E., & Mareev, E. (2014). Recent progress on the global electrical circuit. *Atmospheric Research*, *135*, 208-227.

Yang, J., Zhang, Z., Wei, C., Lu, F., & Guo, Q. (2017). Introducing the new generation of Chinese Geostationary Weather Satellites, Fengyun-4. *Bulletin of the American Meteorological Society*, **98**(8), 1637– 1658. https://doi.org/10.1175/BAMS-D-16-0065.1

Zipser, E. J., D. J. Cecil, C. Liu, S. W. Nesbitt, and D. P. Yorty (2006). Where are the most intense thunderstorms on Earth?, *Bull. Am. Meteorol. Soc*., 87, 1057–1071, doi:10.1175/BAMS-87-8-1057.

817 **Table 1.** LIS and OTD total flash counts, non-fatal flash counts, and non-fatal flash percentages
818 corrected for instrument Detection Efficiency.
819

Instrument	DE-Corrected Flash Count	Non-Fatal Flashes DE-Corrected Flash Count	Non-Fatal Percent of Total Flash Count
OTD	9313438	9140203	98.14
TRMM-LIS	26046715	26033164	99.95
ISS-LIS	3304510	3303107	99.96

820
821

822 **Table 2.** The top 10 Flash Extent Density hotspots for each continent. The ranks and locations of
823 the hotspot grid cell are listed as well as the nearest named place and the distance from the grid
824 cell.
825

Rank	Hotspot Grid Cell			Nearest Place			Distance [km]
	FED [fl/day]	Lat	Lon	Place Name	Admin 1	Country	
				North America			
11	217	14.39	-91.37	Rio Bravo	Suchitepeque	Guatemala	6
28	178	13.04	-87.25	El Obraje	Choluteca	Honduras	18
33	175	22.22	-84.33	Mantua	Pinar del Rio	Cuba	9
38	173	22.85	-82.28	Quivican	Mayabeque	Cuba	8
61	155	21.32	-78.21	Vertientes	Camaguey	Cuba	9
65	153	18.98	-72.19	Mirebalais	Centre	Haiti	19
69	153	22.31	-80.69	Abreus	Cienfuegos	Cuba	13
83	145	22.22	-105.32	La Presa	Nayarit	Mexico	16
91	144	18.08	-77.78	Lacovia	St. Elizabeth	Jamaica	3
92	143	18.26	-67.06	Espino	Anasco	Puerto Rico	7
				South America			
1	389	9.62	-71.80	San Carlos del Zulia (Lake Maracaibo)	Zulia	Venezuela	70
5	274	9.08	-72.96	Tibu	Norte de Santander	Colombia	55
7	249	7.55	-75.40	Caceres	Antioquia	Colombia	6
10	223	5.76	-75.03	Argelia	Antioquia	Colombia	12
12	212	8.27	-74.71	Nechi	Antioquia	Colombia	21
39	172	7.55	-76.31	Mutata	Antioquia	Colombia	37
40	171	-17.27	-65.18	Chimore	Cochabamba	Bolivia	36
47	164	5.49	-76.72	El Canton de San Pablo	Choco	Colombia	16
49	163	7.10	-74.24	Remedios	Antioquia	Colombia	34
55	158	11.15	-72.98	Barrancas	La Guajira	Colombia	30
				Europe			
564	82	45.87	9.17	Pognana Lario	Lombardy	Italy	1
804	72	40.39	13.58	Forio	Campania	Italy	43
862	70	41.37	2.52	Mataro	Catalonia	Spain	20
863	70	40.30	18.99	Orikum	Vlore	Albania	41
1257	59	43.17	17.39	Vrgorac	Splitsko-Dalmatinska	Croatia	4
1339	58	44.34	19.12	Mali Zvornik	Central Serbia	Serbia	4
1427	56	45.69	11.72	Tezze	Veneto	Italy	1
1592	54	37.96	17.91	Capo Rizzuto	Calabria	Italy	127
1597	54	45.60	10.41	Vallio Terme	Lombardy	Italy	2
1618	53	41.37	18.46	Materdomini	Apulia	Italy	90
				Africa			
2	369	-1.98	27.63	Kabare	South Kivu	D.R. Congo	141
3	315	-1.17	28.16	Sake	Nord Kivu	D.R. Congo	108
4	314	-2.97	27.83	Kabare	South Kivu	D.R. Congo	119
6	254	-0.27	28.24	Butembo	Nord Kivu	D.R. Congo	125
8	240	-2.61	26.92	Kampene	Maniema	D.R. Congo	113
9	227	-0.90	27.17	Sake	Nord Kivu	D.R. Congo	222
13	204	4.41	8.48	Ikang	Cross River	Nigeria	43
14	201	0.36	20.33	Boende	Equateur	D.R. Congo	94
15	199	-1.62	20.88	Boende	Equateur	D.R. Congo	149
17	194	-0.18	21.32	Boende	Equateur	D.R. Congo	50

				Asia			
16	198	3.06	101.60	Subang Jaya	Selangor	Malaysia	3
22	182	34.36	72.35	Daggar	Khyber Pakhtunkhwa	Pakistan	21
25	180	1.62	103.75	Ulu Tiram	Johor	Malaysia	8
27	179	3.69	98.06	Bambol	Aceh	Indonesia	33
32	176	33.19	74.48	Rajaori	Kashmir	India	26
41	167	33.73	70.73	Doaba	Khyber Pakhtunkhwa	Pakistan	34
43	165	3.15	100.62	Kampung Tanjung Karang	Selangor	Malaysia	70
48	164	3.96	101.07	Teluk Intan	Perak	Malaysia	9
53	161	-6.66	106.68	Ciampea	West Java	Indonesia	12
66	153	25.18	91.84	Cherrapunji	Meghalaya	India	19
				Oceania			
170	120	-15.38	125.29	Derby	Western Australia	Australia	277
199	116	-4.77	142.88	Ambunti	East Sepik	Papua New Guinea	62
298	103	-16.37	125.62	Derby	Western Australia	Australia	236
311	101	-16.64	124.67	Derby	Western Australia	Australia	133
318	100	-7.11	145.12	Ihu	Gulf	Papua New Guinea	93
343	98	-14.84	126.18	Kununurra	Western Australia	Australia	294
351	96	-15.47	129.82	Kununurra	Western Australia	Australia	120
408	92	-4.86	143.98	Wabag	Enga	Papua New Guinea	76
441	89	-5.40	145.01	Minj	Jiwaka	Papua New Guinea	67
548	83	-15.65	128.44	Kununurra	Western Australia	Australia	36

826
827

828 **Table 3.** The top 10 Thunderstorm Duty (percentage of total viewtime with lightning) hotspots
829 for each continent. The ranks and locations of the hotspot grid cell are listed as well as the
830 nearest named place and the distance from the grid cell.
831

Rank	Hotspot Grid Cell			Nearest Place			Distance [km]
	Duty [% VT]	Lat	Lon	Place Name	Admin 1	Country	
				North America			
17	4.33	14.30	-91.06	Santa Lucia Cotzumalguapa	Escuintla	Guatemala	6
29	4.01	14.66	-91.95	Flores Costa Cuca	Quetzaltenango	Guatemala	10
109	3.14	9.08	-79.70	Santa Clara	Panama	Panama	8
119	3.10	7.10	-78.13	Jurado	Choco	Colombia	41
122	3.09	19.07	-100.21	San Pedro Tenayac	Mexico	Mexico	4
128	3.07	15.29	-92.78	Jiquilpan (Estacion Bonanza)	Chiapas	Mexico	7
134	3.04	8.00	-77.93	Camoganti	Darien	Panama	6
144	3.00	19.43	-104.44	La Resolana	Jalisco	Mexico	20
147	2.99	16.01	-88.99	Punta Gorda	Toledo	Belize	22
152	2.97	17.18	-94.33	La Chinantla	Veracruz	Mexico	17
				South America			
4	6.05	9.53	-71.87	San Carlos del Zulia	Zulia	Venezuela	60
7	5.24	5.49	-75.09	Pensilvania	Caldas	Colombia	14
8	5.13	9.17	-73.07	La Jagua de Ibirico	Cesar	Colombia	52
9	5.10	5.58	-76.55	Lloro	Choco	Colombia	9
12	4.79	7.46	-75.57	Valdivia	Antioquia	Colombia	27
13	4.75	8.09	-74.68	Nechi	Antioquia	Colombia	11
21	4.26	7.02	-76.76	Murindo	Antioquia	Colombia	3
23	4.22	4.59	-76.79	Novita	Choco	Colombia	46
27	4.04	6.03	-73.35	Suaita	Santander	Colombia	13
30	3.99	6.75	-74.09	Puerto Parra	Santander	Colombia	11
				Europe			
1043	1.69	45.78	9.03	Villa Guardia	Lombardy	Italy	1
1478	1.46	45.87	10.46	Bagolino	Lombardy	Italy	5
1545	1.42	42.18	19.66	Nicaj-Shosh	Shkoder	Albania	10
1647	1.38	39.22	21.13	Ano Kalentini	Epirus	Greece	6
1682	1.36	40.83	20.09	Tunje	Elbasan	Albania	2
1754	1.34	38.68	15.55	San Nicolo	Calabria	Italy	26
1847	1.30	37.51	21.32	Pyrgos	West Greece	Greece	22
2034	1.24	42.45	12.92	Cantalice	Latium	Italy	2
2103	1.22	45.87	12.14	Sernaglia della Battaglia	Veneto	Italy	1
2142	1.20	43.26	17.79	Rodoc	Federation of Bosnia and Herzegovina	Bosnia and Herzegovina	6
				Africa			
1	7.29	-1.89	27.63	Kabare	South Kivu	D.R. Congo	146
2	6.18	-1.26	28.34	Sake	Nord Kivu	D.R. Congo	86
3	6.13	-2.97	28.10	Kabare	South Kivu	D.R. Congo	93
5	5.44	-0.36	28.33	Butembo	Nord Kivu	D.R. Congo	120
6	5.27	-0.81	27.53	Sake	Nord Kivu	D.R. Congo	189
10	5.05	4.32	8.75	Bamusso	South-West Province	Cameroon	23
11	4.89	-2.16	28.53	Kabare	South Kivu	D.R. Congo	47
15	4.48	-2.79	27.20	Kampene	Maniema	D.R. Congo	107

18	4.33	-1.44	26.81	Kindu	Maniema	D.R. Congo	194
20	4.30	-3.87	28.22	Uvira	South Kivu	D.R. Congo	115
				Asia			
14	4.56	3.15	100.62	Kampung Tanjung Karang	Selangor	Malaysia	70
16	4.36	3.60	98.05	Bambol	Aceh	Indonesia	25
19	4.32	2.97	101.60	Subang Jaya	Selangor	Malaysia	9
22	4.22	-6.75	106.51	Kubang	Banten	Indonesia	5
28	4.04	-7.20	109.25	Baturaden	Central Java	Indonesia	12
35	3.77	1.35	103.65	Johor Bahru	Johor	Malaysia	18
37	3.77	4.95	100.67	Simpang Empat	Perak	Malaysia	4
39	3.74	3.87	99.98	Lumut	Perak	Malaysia	83
43	3.71	2.07	101.53	Titiakar	Riau	Indonesia	7
44	3.70	4.05	101.08	Teluk Intan	Perak	Malaysia	7
				Oceania			
48	3.67	-4.77	142.97	Ambunti	East Sepik	Papua New Guinea	64
90	3.25	-4.86	143.89	Wabag	Enga	Papua New Guinea	72
97	3.23	-7.11	145.03	Ihu	Gulf	Papua New Guinea	97
160	2.92	-4.68	141.87	Ambunti	East Sepik	Papua New Guinea	117
213	2.74	-5.40	144.92	Minj	Jiwaka	Papua New Guinea	62
421	2.33	-7.83	146.36	Kerema	Gulf	Papua New Guinea	66
483	2.22	-6.57	155.28	Panguna	Bougainville	Papua New Guinea	36
506	2.19	-5.76	149.89	Kimbe	West New Britain	Papua New Guinea	36
518	2.18	-8.64	147.66	Kokoda	Northern Province	Papua New Guinea	28
531	2.16	-4.68	152.07	Kokopo	East New Britain	Papua New Guinea	42
48	3.67	-4.77	142.97	Ambunti	East Sepik	Papua New Guinea	64

832
833

834 **Table 4.** The top 10 national capital cities by Flash Extent Density and Thunderstorm Duty.
835

Rank	FED [fl/day]	Duty [% VT]	Lat	Lon	Name	Country
Top 10 Capital Cities by Flash Extent Density						
1	179	4.21	3.17	101.70	Kuala Lumpur	Malaysia
2	158	2.13	33.68	73.05	Islamabad	Pakistan
3	138	3.39	1.28	103.85	Singapore	Singapore
4	127	1.99	23.12	-82.35	Havana	Cuba
5	106	2.66	8.97	-79.53	Panama City	Panama
6	99	2.48	13.75	100.52	Bangkok	Thailand
7	96	2.34	14.60	120.97	Manila	Philippines
8	95	2.31	6.92	79.83	Colombo	Sri Lanka
9	95	1.48	23.72	90.40	Dhaka	Bangladesh
10	87	2.10	4.37	18.58	Bangui	Central African Republic
Top 10 Capital Cities by Thunderstorm Duty						
1	179	4.21	3.17	101.70	Kuala Lumpur	Malaysia
2	138	3.39	1.28	103.85	Singapore	Singapore
3	106	2.66	8.97	-79.53	Panama City	Panama
4	84	2.60	-6.17	106.82	Jakarta	Indonesia
5	99	2.48	13.75	100.52	Bangkok	Thailand
6	80	2.39	13.70	-89.20	San Salvador	El Salvador
7	60	2.37	9.03	38.70	Addis Ababa	Ethiopia
8	96	2.34	14.60	120.97	Manila	Philippines
9	95	2.31	6.92	79.83	Colombo	Sri Lanka
10	78	2.28	0.38	9.45	Libreville	Gabon

836
837
838
839

840 **Table 5.** The top 10 major airports by Flash Extent Density and Thunderstorm Duty.
841

Rank	FED [fl/day]	Duty [% VT]	Lat	Lon	IATA Code	Name	City	Country
Top 10 Major Airports by Flash Extent Density								
1	151	2.34	22.99	-82.41	HAV	Jose Marti International Airport	Havana	Cuba
2	139	3.73	2.75	101.71	KUL	Kuala Lumpur International Airport	Kuala Lumpur	Malaysia
3	113	3.15	1.35	103.99	SIN	Singapore Changi Airport	Singapore	Singapore
4	108	2.55	9.07	-79.38	PTY	Tocumen International Airport	Tocumen	Panama
5	105	2.03	26.54	-81.76	RSW	Southwest Florida International Airport	Fort Myers	United States
6	96	2.18	14.51	121.02	MNL	Ninoy Aquino International Airport	Manila	Philippines
7	91	2.81	4.87	8.09	QUO	Akwa Ibom International Airport	Uyo	Nigeria
8	90	1.58	33.55	72.83	ISB	Islamabad International Airport	Islamabad	Pakistan
9	89	2.43	13.91	100.61	DMK	Don Mueang International Airport	Bangkok	Thailand
10	89	2.26	10.82	106.65	SGN	Tan Son Nhat International Airport	Ho Chi Minh City	Vietnam
Top 10 Major Airports by Thunderstorm Duty								
1	139	3.73	2.75	101.71	KUL	Kuala Lumpur International Airport	Kuala Lumpur	Malaysia
2	113	3.15	1.35	103.99	SIN	Singapore Changi Airport	Singapore	Singapore
3	91	2.81	4.87	8.09	QUO	Akwa Ibom International Airport	Uyo	Nigeria
4	86	2.73	-6.13	106.66	CGK	Soekarno-Hatta International Airport	Jakarta	Indonesia
5	108	2.55	9.07	-79.38	PTY	Tocumen International Airport	Tocumen	Panama
6	79	2.48	-7.38	112.79	SUB	Juanda International Airport	Surabaya	Indonesia
7	89	2.43	13.91	100.61	DMK	Don Mueang International Airport	Bangkok	Thailand
8	151	2.34	22.99	-82.41	HAV	Jose Marti International Airport	Havana	Cuba
9	87	2.30	13.44	-89.06	SAL	Monseñor Óscar Arnulfo Romero International Airport	San Salvador	El Salvador
10	89	2.26	10.82	106.65	SGN	Tan Son Nhat International Airport	Ho Chi Minh City	Vietnam

842
843
844
845

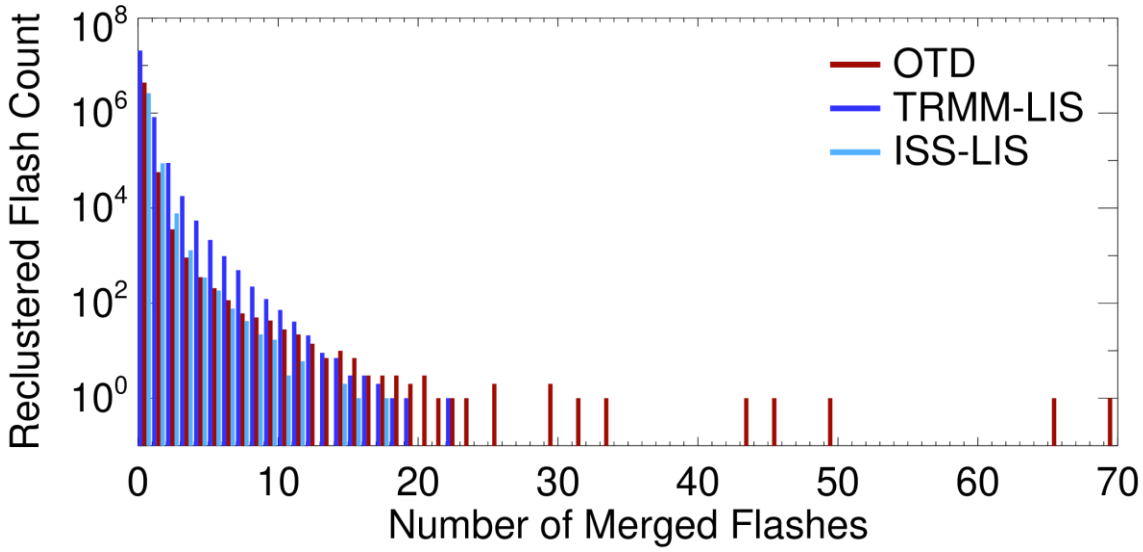

Figure 1. Histograms for the number of LIS and OTD flashes that were merged by our reclustering algorithms. While most of the original LIS and OTD flashes were not modified by reclustering, certain cases were split into tens of flash features by the LIS / OTD clustering algorithms.

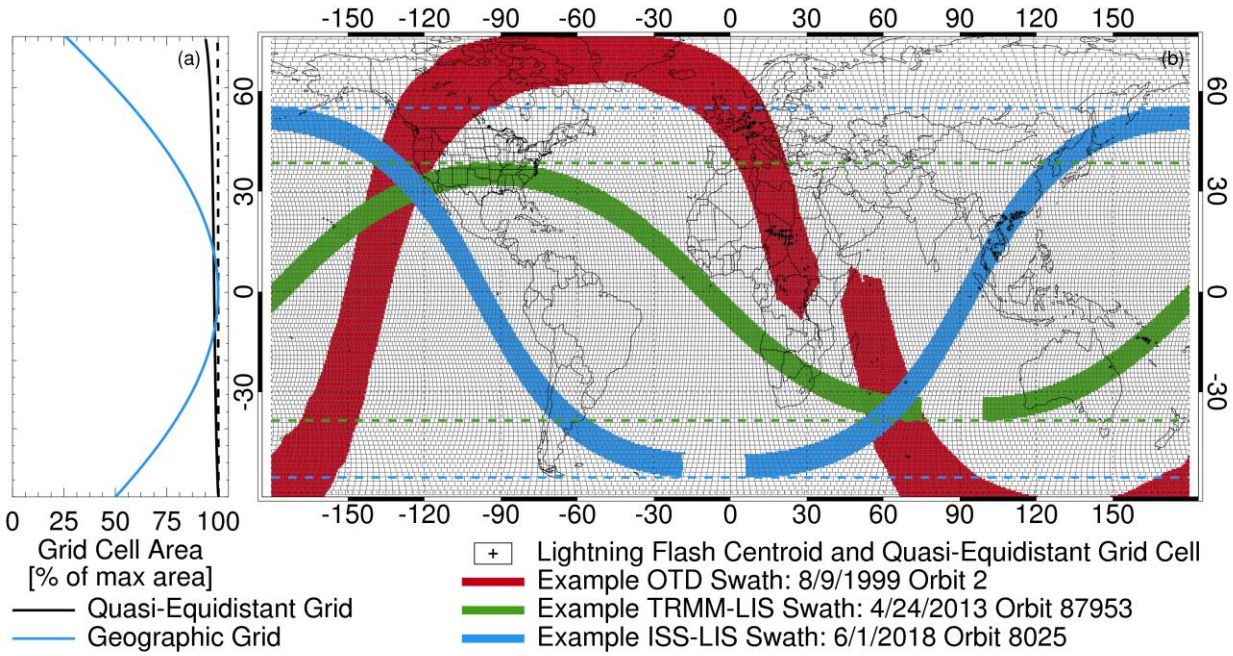

Figure 2. The geometry of the quasi-equidistant grid. (a) Comparison of the latitude distributions of grid cell area for a 150 km (solid black) and 10 km (dashed black) quasi-equidistant grid and a geographic grid (blue). (b) Map showing grid cell boundaries for a 150 km quasi-equidistant grid overlaid on top of example orbital swaths for OTD (red), TRMM-LIS (green), and ISS-LIS (blue). Note that the ISS-LIS orbit number shown will be removed in future versions of the ISS-LIS data, and orbits will be referenced by start and end times, instead. Maximum orbital extents for each instrument are shown as dashed horizontal lines. The locations of lightning flash centroids in each orbit are indicated with + symbols.

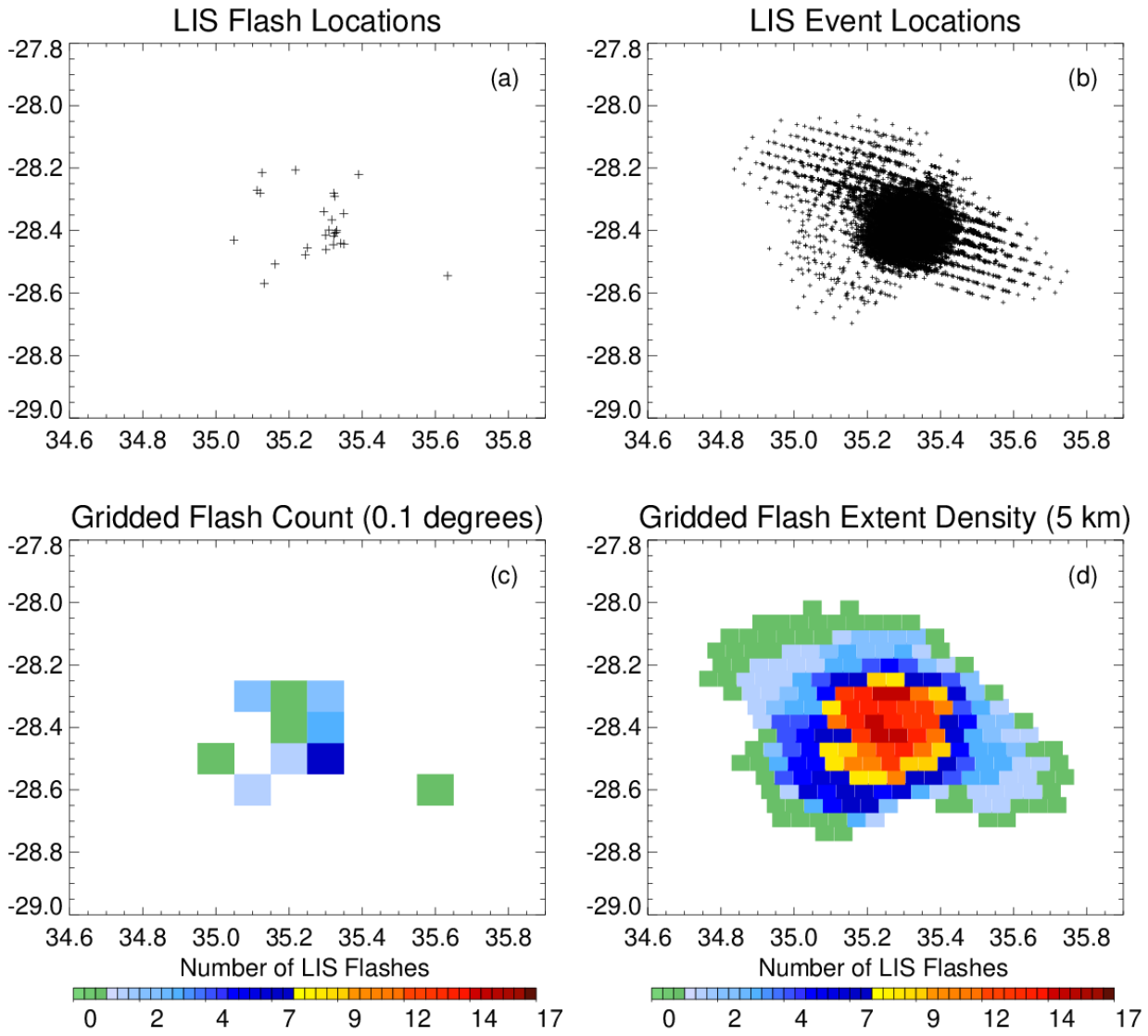

Figure 3. The locations of LIS flashes (a) and events (b) that are gridded to compute FRD (c) and FED (d).

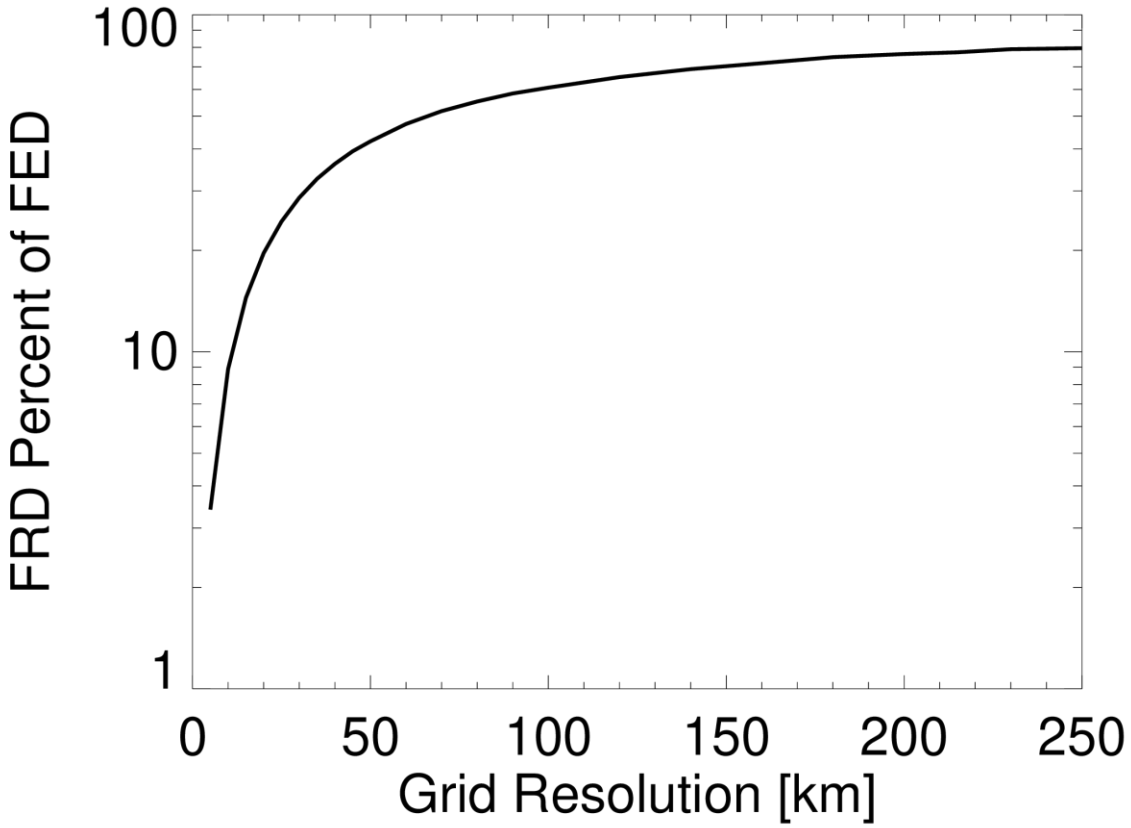

Figure 4. Average FRD fraction of the FED for identical grids whose resolutions vary from 5 km to 250 km from a selection of 1000 TRMM-LIS orbits. For very high resolution grids (5-10 km), the FRD is less than 10% of the FED. For larger grids, the FED and FRD are nearly identical – except in cases where the FED extends over multiple grid points.

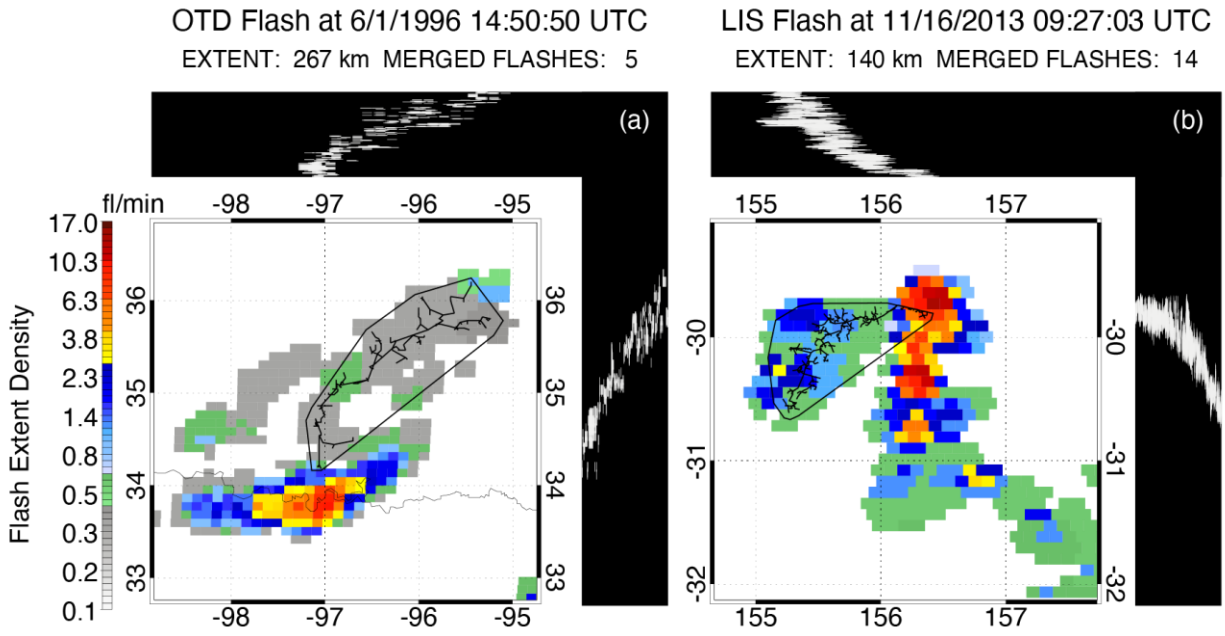

Figure 5. Examples of OTD (a) and LIS (b) megaflash events that were split into 5 (OTD) and 14 (LIS) flash features in the original science datasets. Flash progression is depicted as line segments connecting each group with the nearest preceding group on top of a Flash Extent Density map with a convex hull also overlaid surrounding the flash footprint. The longitude (top) and latitude (right) extent of each sequential group in the flash is also plotted next to the map.

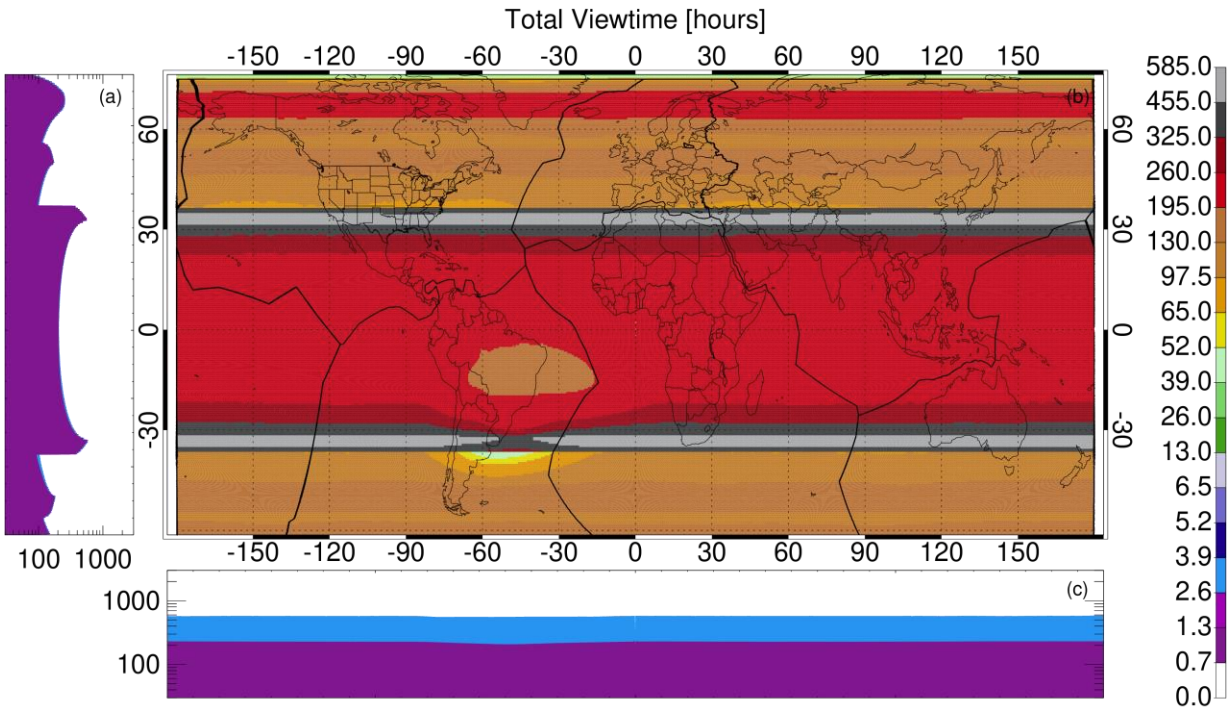

Figure 6. Global distributions of total LIS / OTD viewtime. Total viewtime at each gridpoint is mapped in (b) with political (thin) and continental (thick) boundaries overlaid. Mean (purple) and maximum (blue) viewtimes for each latitude (a) and longitude (c) are also shown to the left of and below the map. Note that because viewtime is largely constant with longitude, the blue maximum curve is nearly indistinguishable from the mean purple curve in (a).

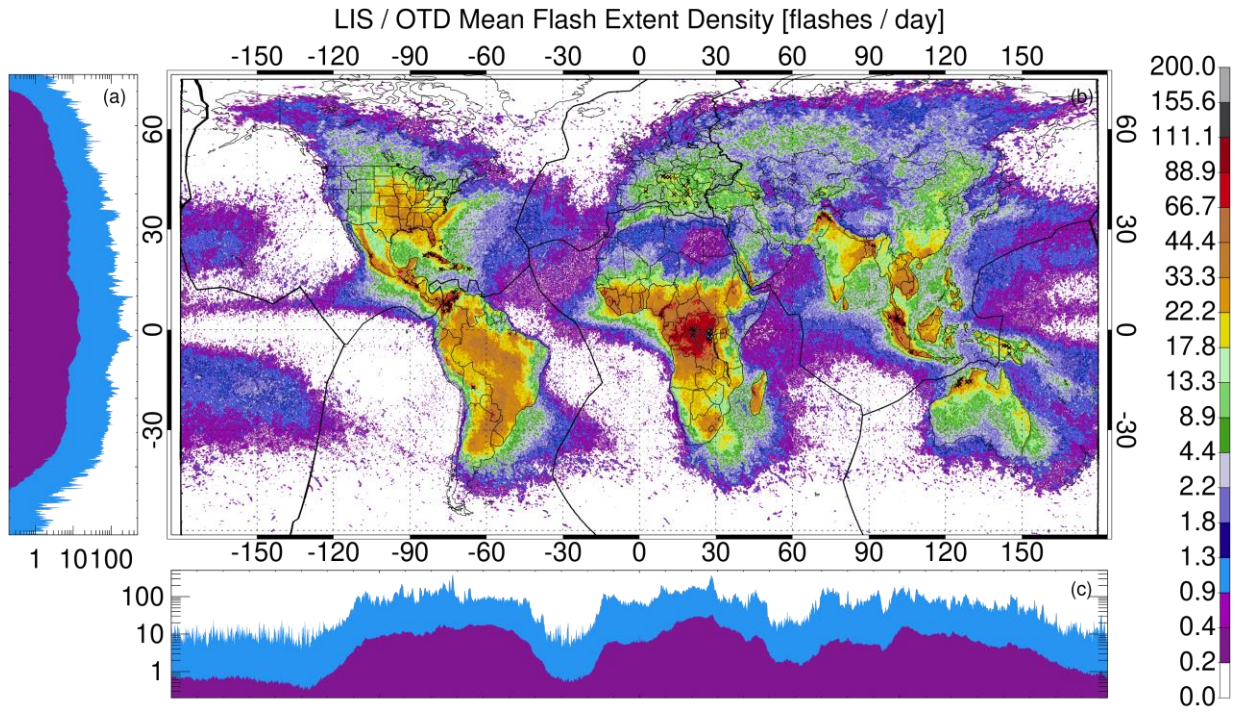

Figure 7. Global distributions of mean LIS / OTD Flash Extent Density plotted following the style of Figure 6. Mean (purple) and maximum (blue) FED values for each latitude (a) and longitude (c) are also shown to the left of and below the map in (b). Since a 10-km grid is used, the units are flashes per day – approximating how many flashes an observer would detect overhead. The top 10 FED hotspot locations for each continent are shown with + symbols.

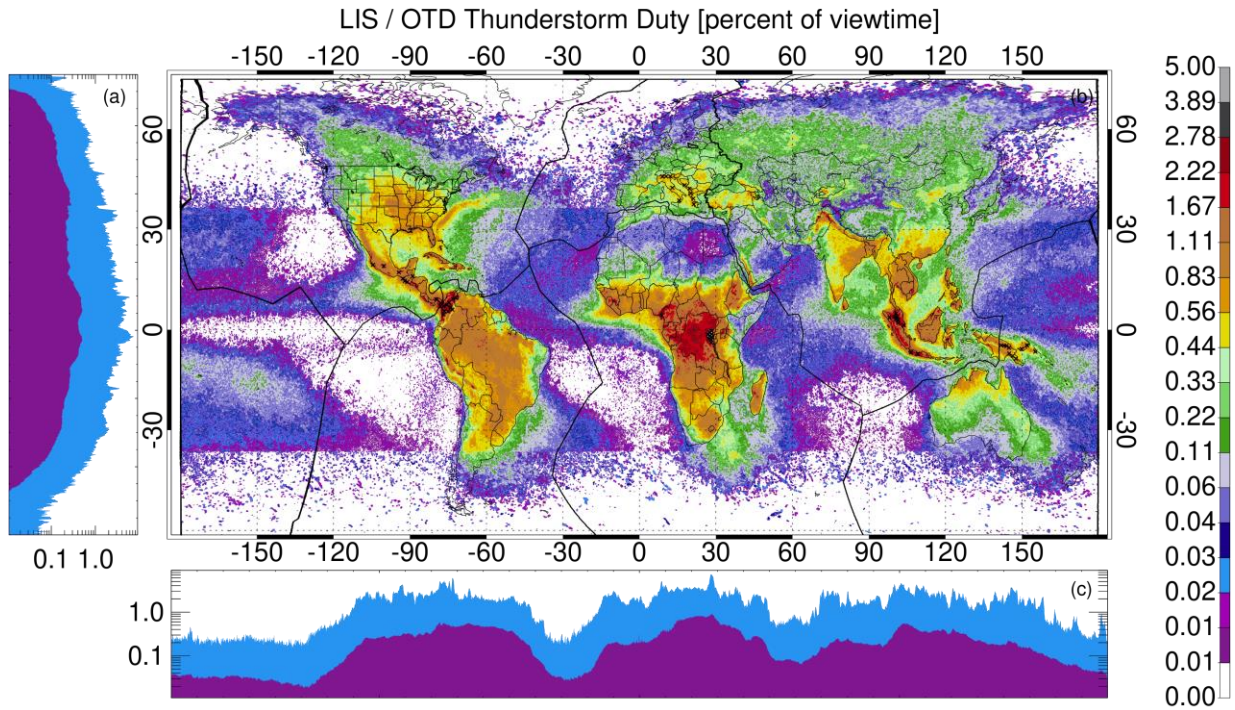

Figure 8. Global distributions of mean LIS / OTD Thunderstorm Duty (percent of the total viewtime where lightning is detected) plotted in the style of Figure 6. Mean (purple) and maximum (blue) duty values for each latitude (a) and longitude (c) are also shown to the left of and below the map in (b). The top 10 duty hotspot locations for each continent are shown with + symbols.

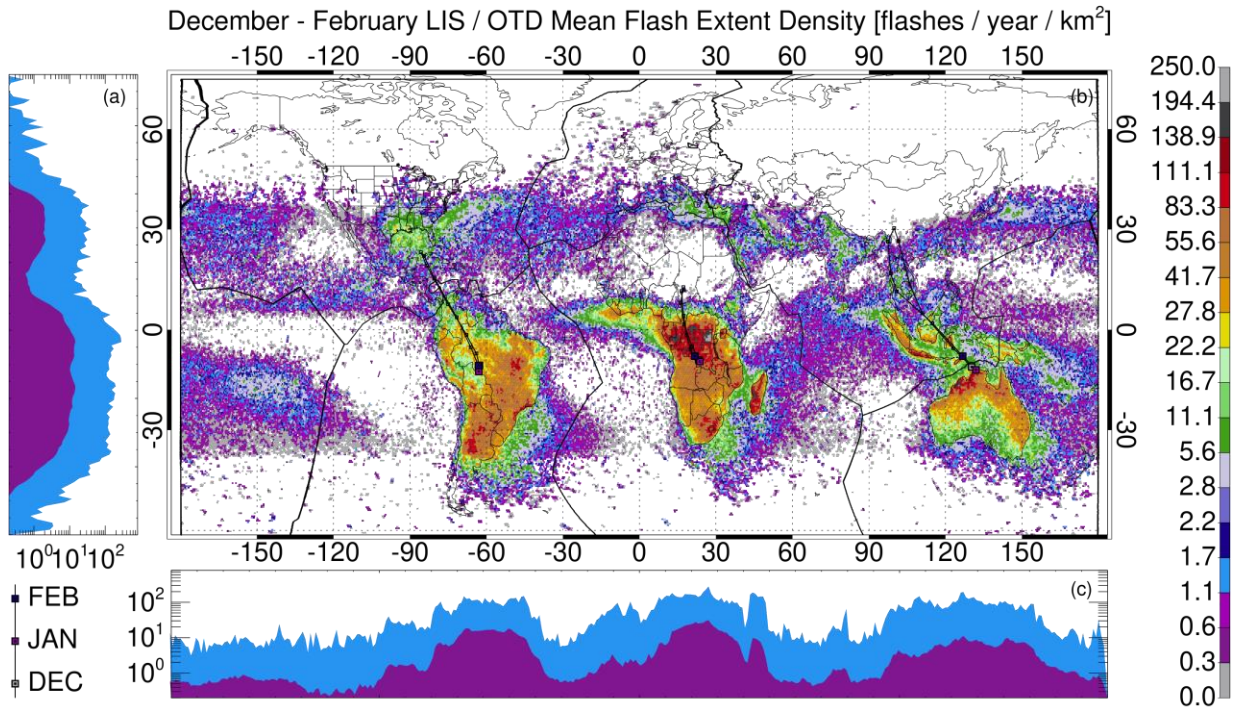

Figure 9. Global distributions of December – February mean LIS / OTD Flash Extent Density plotted following the style of Figure 6. Mean (purple) and maximum (blue) FED values for each latitude (a) and longitude (c) are also shown to the left of and below the map in (b). Since a coarse 50-km grid is used, the units are flashes per day per square kilometer. The annual circuit traversed by the center of lightning for each primary chimney region (the Americas, Europe and Africa, and Asia and Oceania) is plotted as a line contour with box symbols representing each of the 12 months. Large colored boxes are shown for the season depicted in the contour plot.

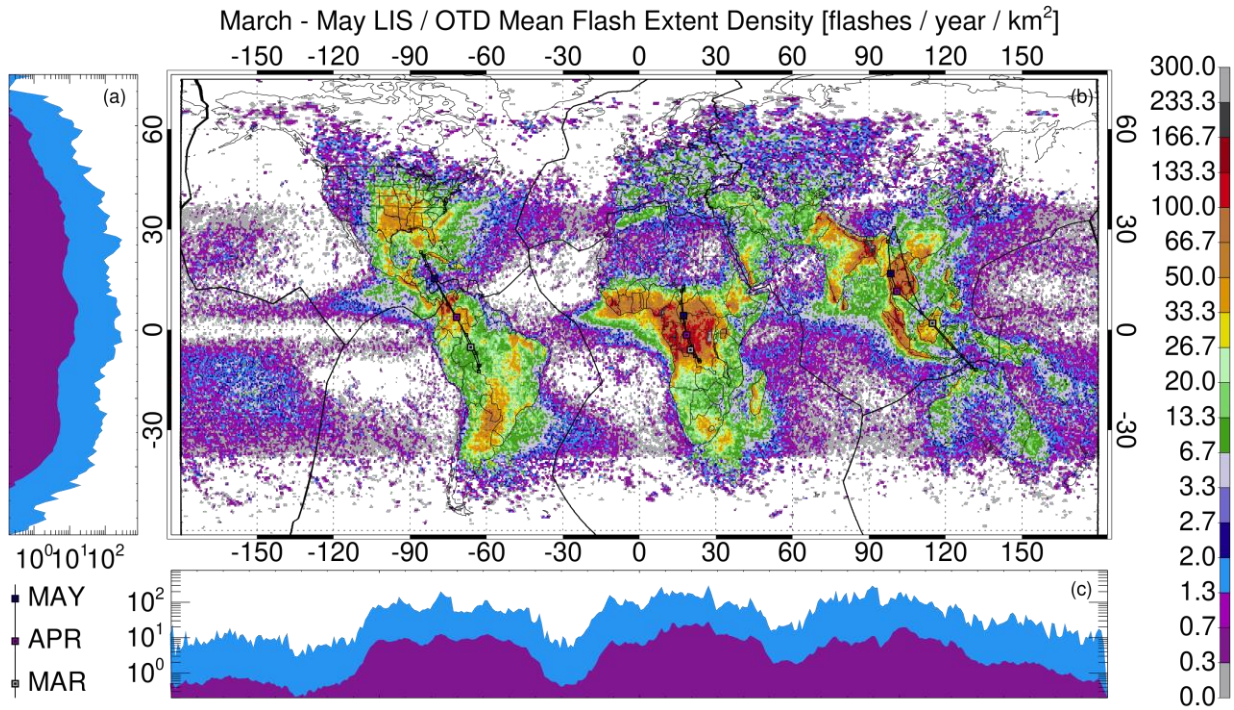

Figure 10. As in Figure 9, but for March - May. Mean (purple) and maximum (blue) FED values for each latitude (a) and longitude (c) are also shown to the left of and below the map in (b).

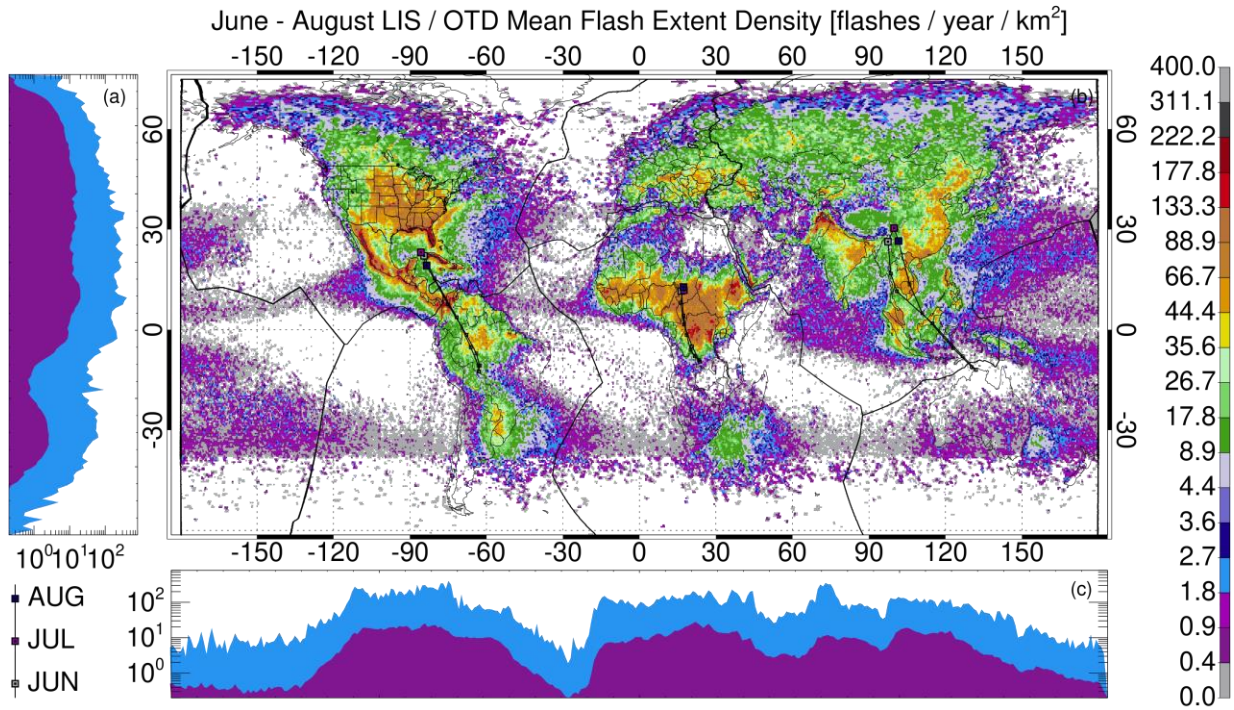

Figure 11. As in Figure 9, but for June - August. Mean (purple) and maximum (blue) FED values for each latitude (a) and longitude (c) are also shown to the left of and below the map in (b).

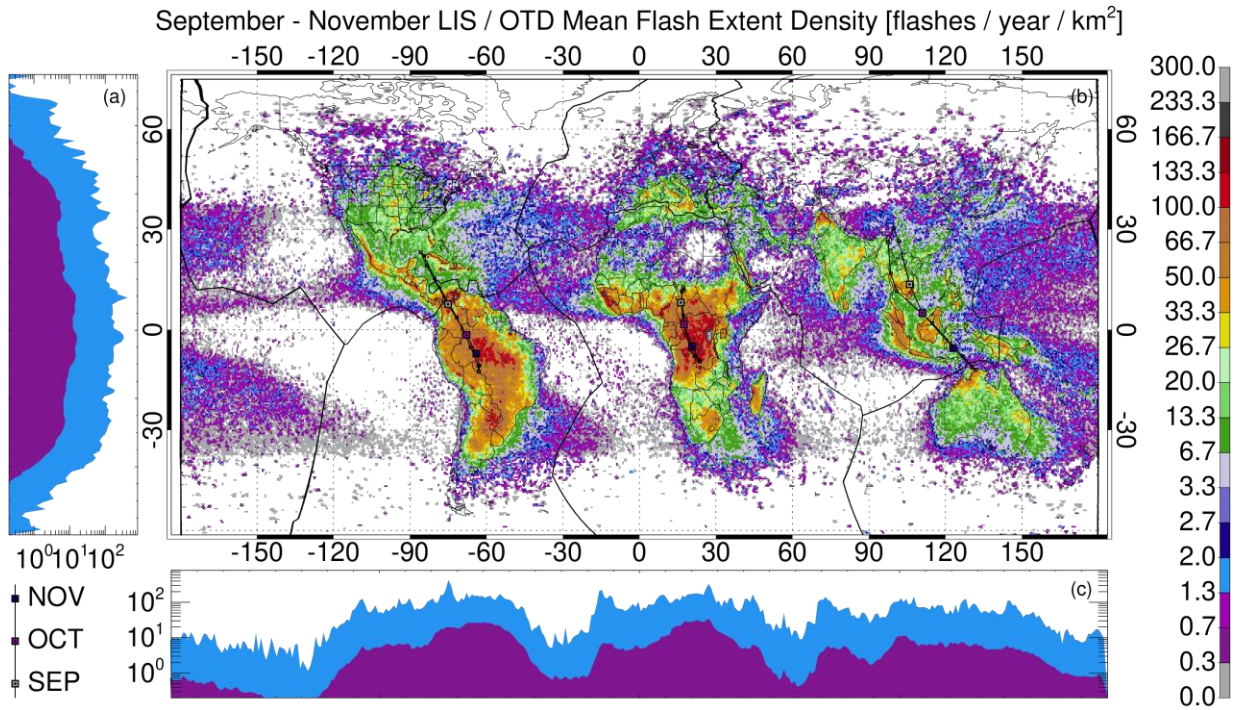

Figure 12. As in Figure 9, but for September - November. Mean (purple) and maximum (blue) FED values for each latitude (a) and longitude (c) are also shown to the left of and below the map in (b).

Figure 1.

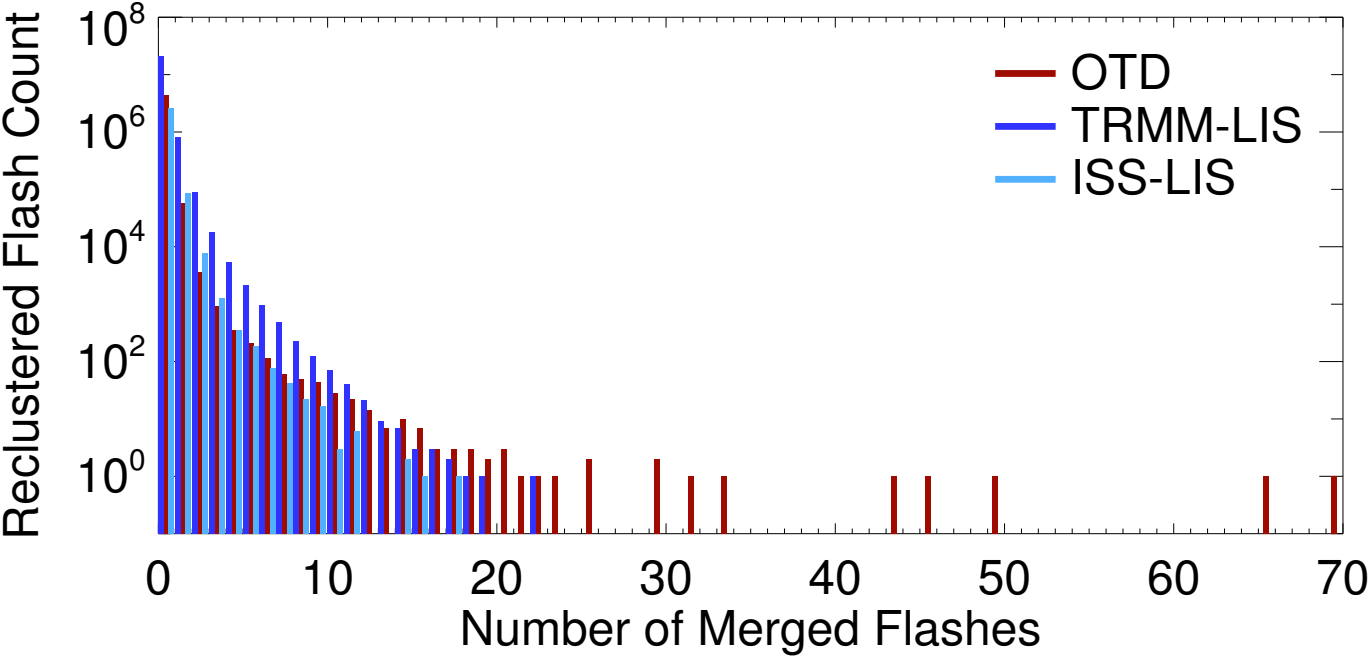
Reclustered Flash Count
10^8
10^6
10^4
10^2
10^0
OTD
TRMM-LIS
ISS-LIS
0
10
20
30
40
50
60
70
Number of Merged Flashes

Figure 2.

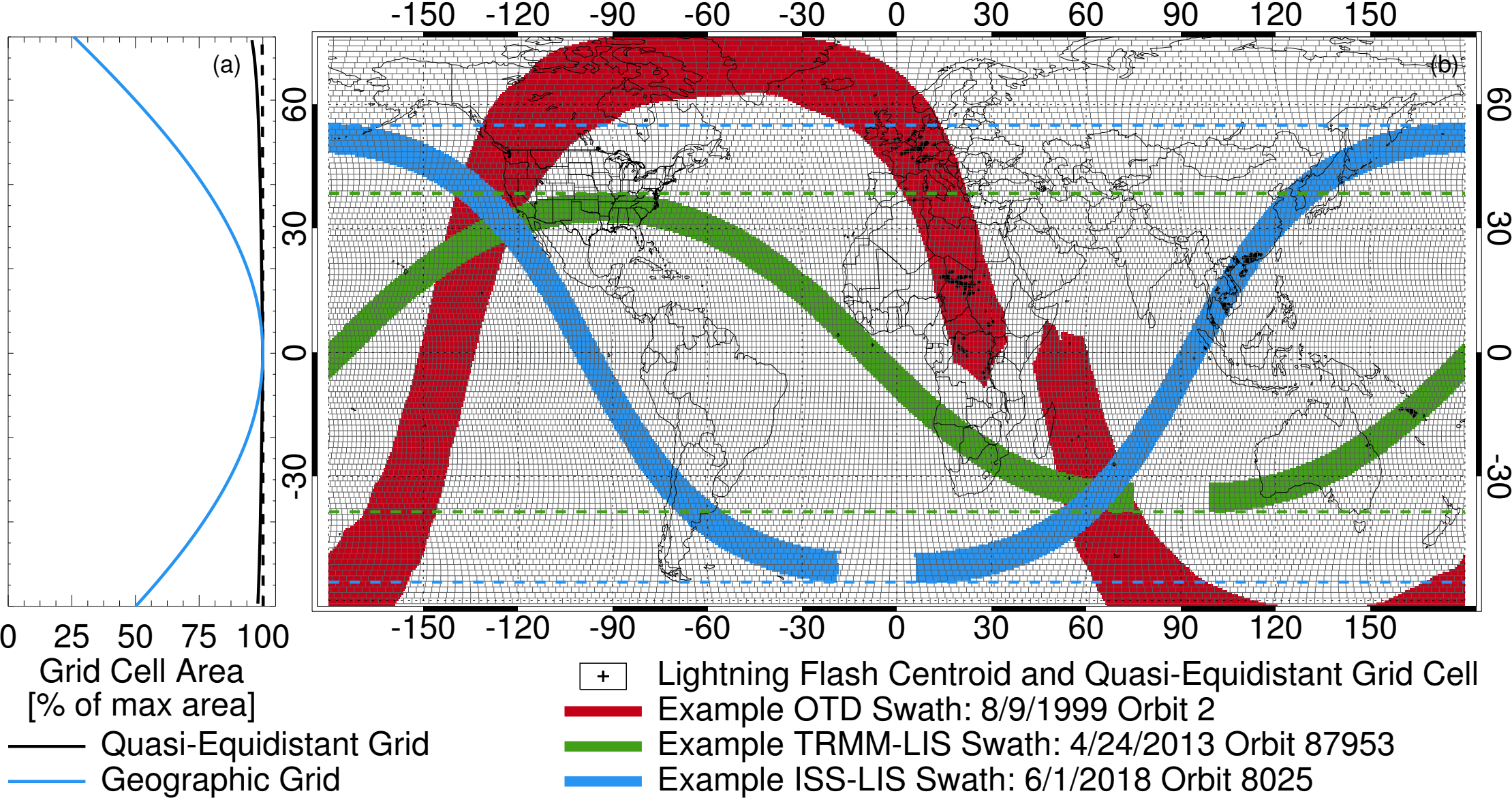
(a)
(b)
-150 -120 -90 -60 -30 0 30 60 90 120 150
60
30
0
-30
0 25 50 75 100
Grid Cell Area
[% of max area]
Quasi-Equidistant Grid
Geographic Grid
Lightning Flash Centroid and Quasi-Equidistant Grid Cell
Example OTD Swath: 8/9/1999 Orbit 2
Example TRMM-LIS Swath: 4/24/2013 Orbit 87953
Example ISS-LIS Swath: 6/1/2018 Orbit 8025

Figure 3.

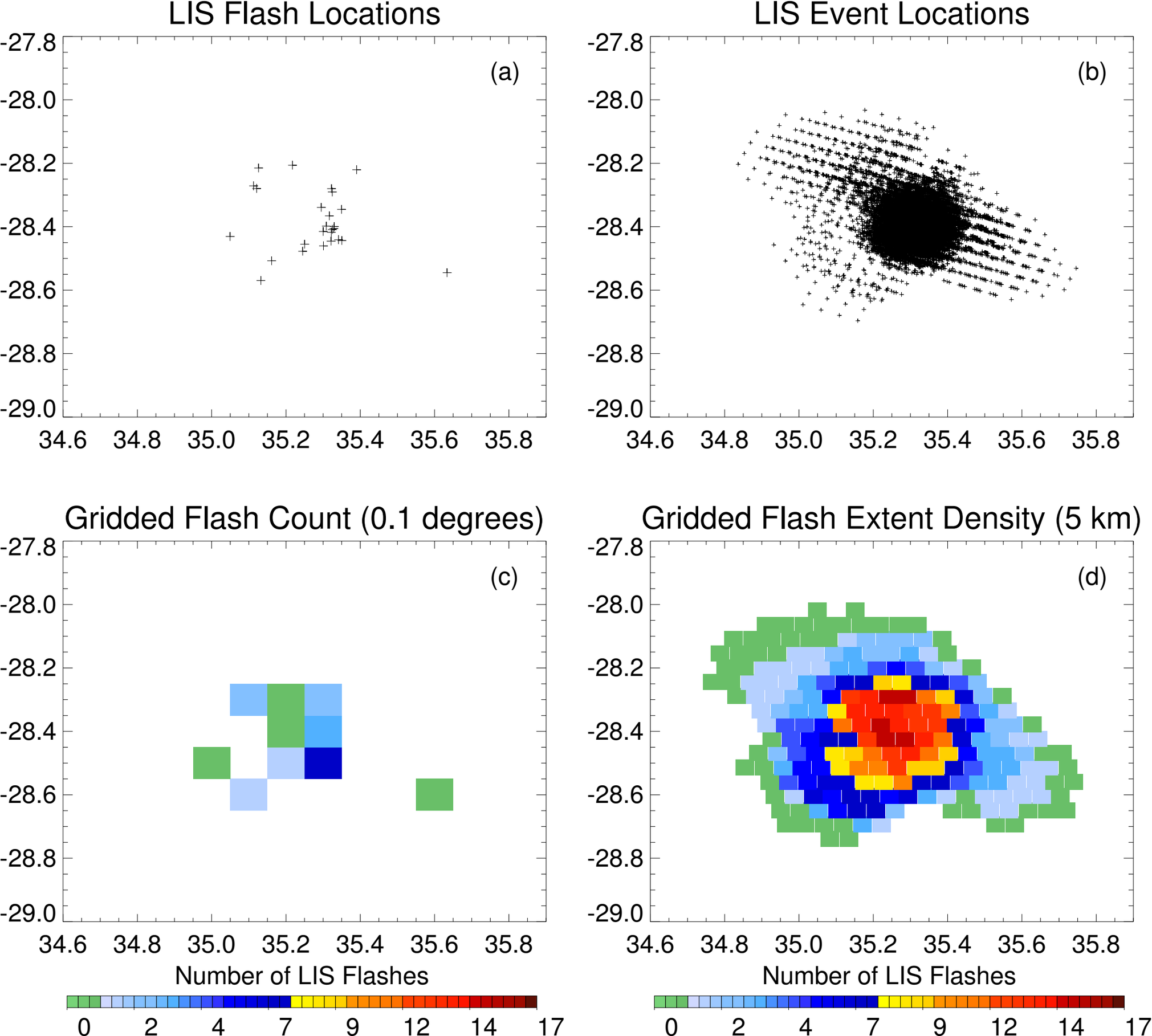
LIS Flash Locations
(a)
LIS Event Locations
(b)
Gridded Flash Count (0.1 degrees)
(c)
Gridded Flash Extent Density (5 km)
(d)
-27.8
-28.0
-28.2
-28.4
-28.6
-28.8
-29.0
34.6
34.8
35.0
35.2
35.4
35.6
35.8
Number of LIS Flashes
0
2
4
7
9
12
14
17

Figure 4.

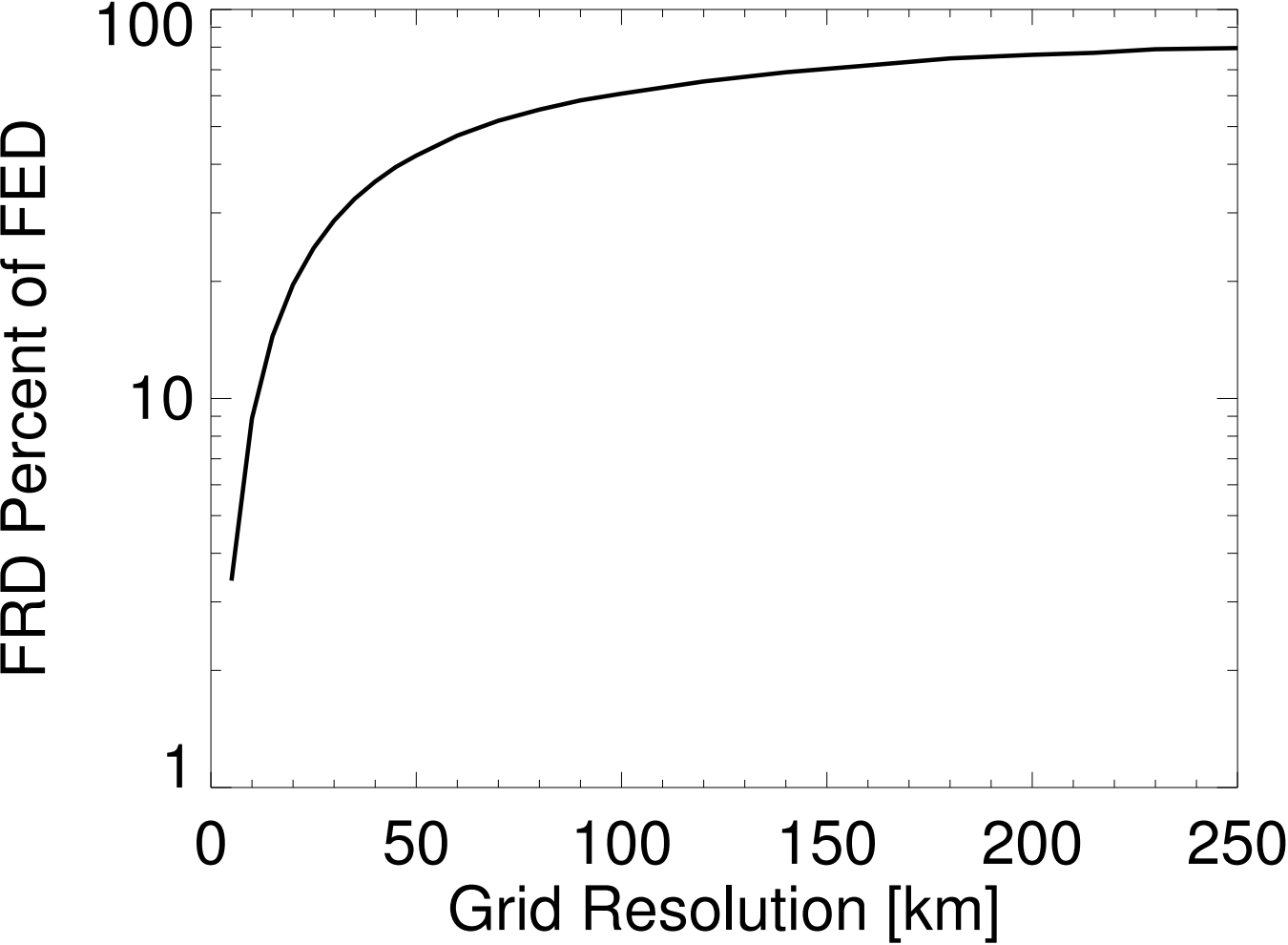
100
10
1
FRD Percent of FED
0
50
100
150
200
250
Grid Resolution [km]

Figure 5.

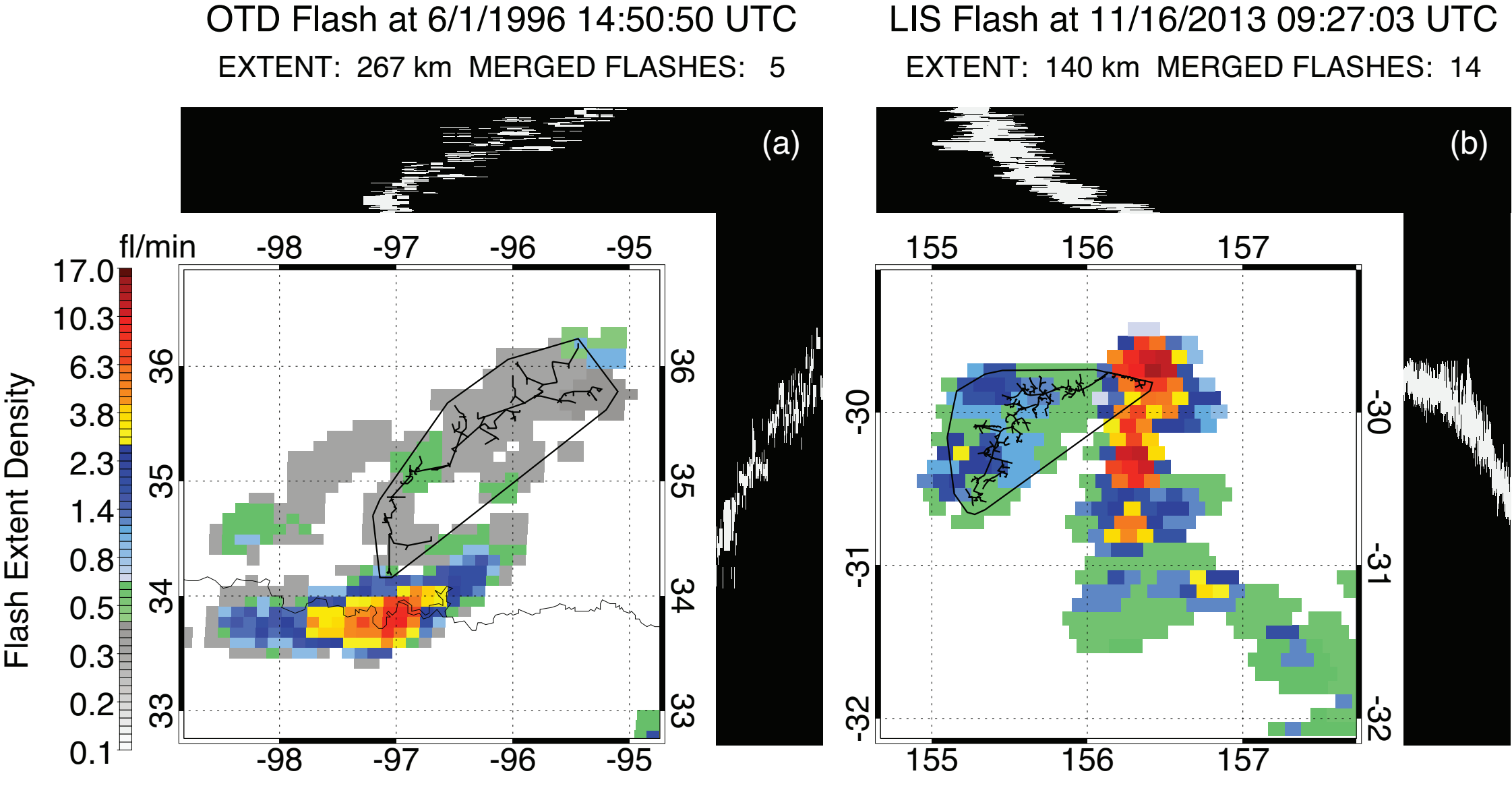
OTD Flash at 6/1/1996 14:50:50 UTC
EXTENT: 267 km MERGED FLASHES: 5
LIS Flash at 11/16/2013 09:27:03 UTC
EXTENT: 140 km MERGED FLASHES: 14
(a)
(b)
fl/min
Flash Extent Density
17.0
10.3
6.3
3.8
2.3
1.4
0.8
0.5
0.3
0.2
0.1
-98
-97
-96
-95
36
35
34
33
155
156
157
-30
-31
-32

Figure 6.

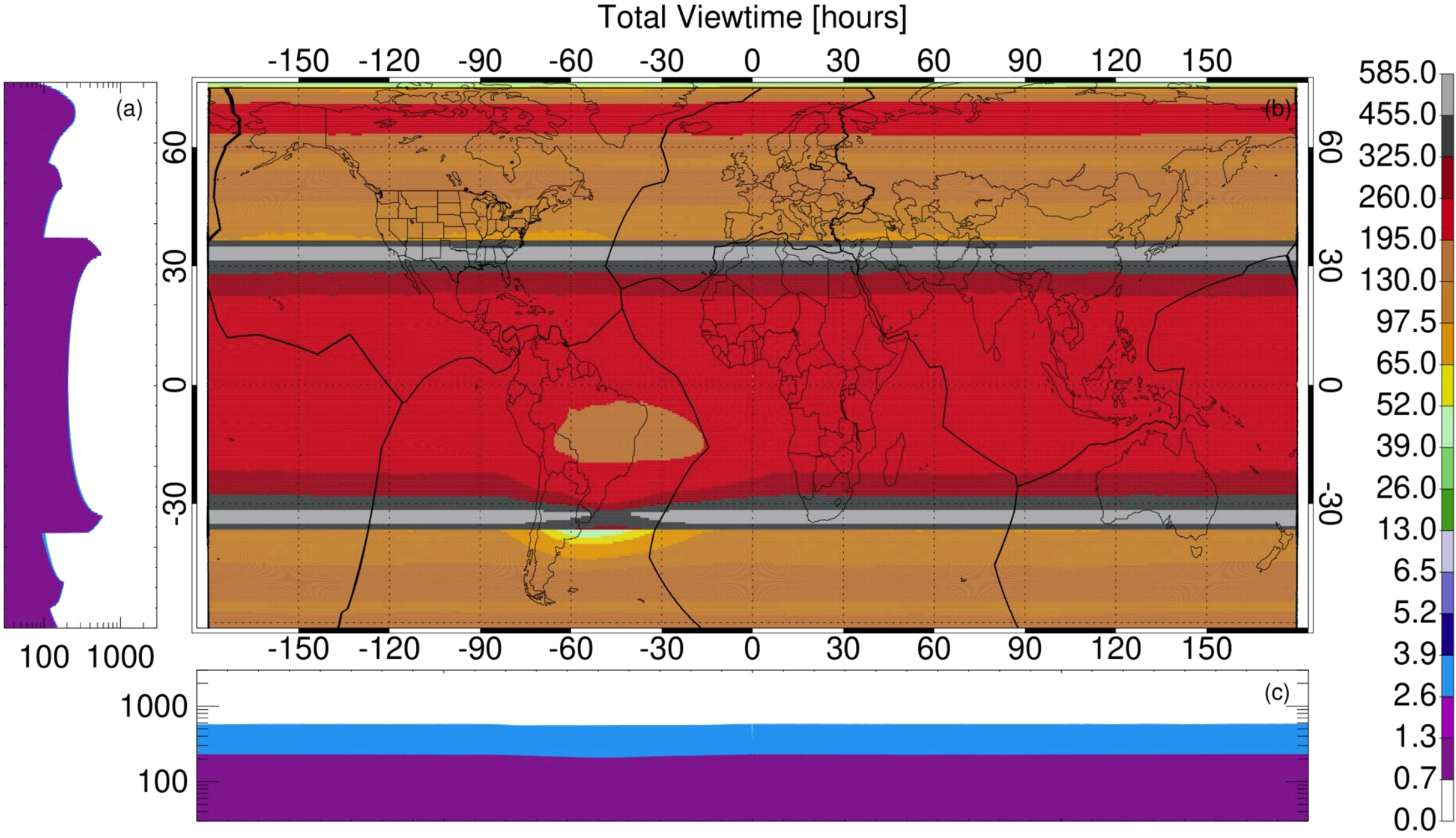
Total Viewtime [hours]
(a)
(b)
(c)
100
1000
-150
-120
-90
-60
-30
0
30
60
90
120
150
60
30
0
-30
585.0
455.0
325.0
260.0
195.0
130.0
97.5
65.0
52.0
39.0
26.0
13.0
6.5
5.2
3.9
2.6
1.3
0.7
0.0

Figure 7.

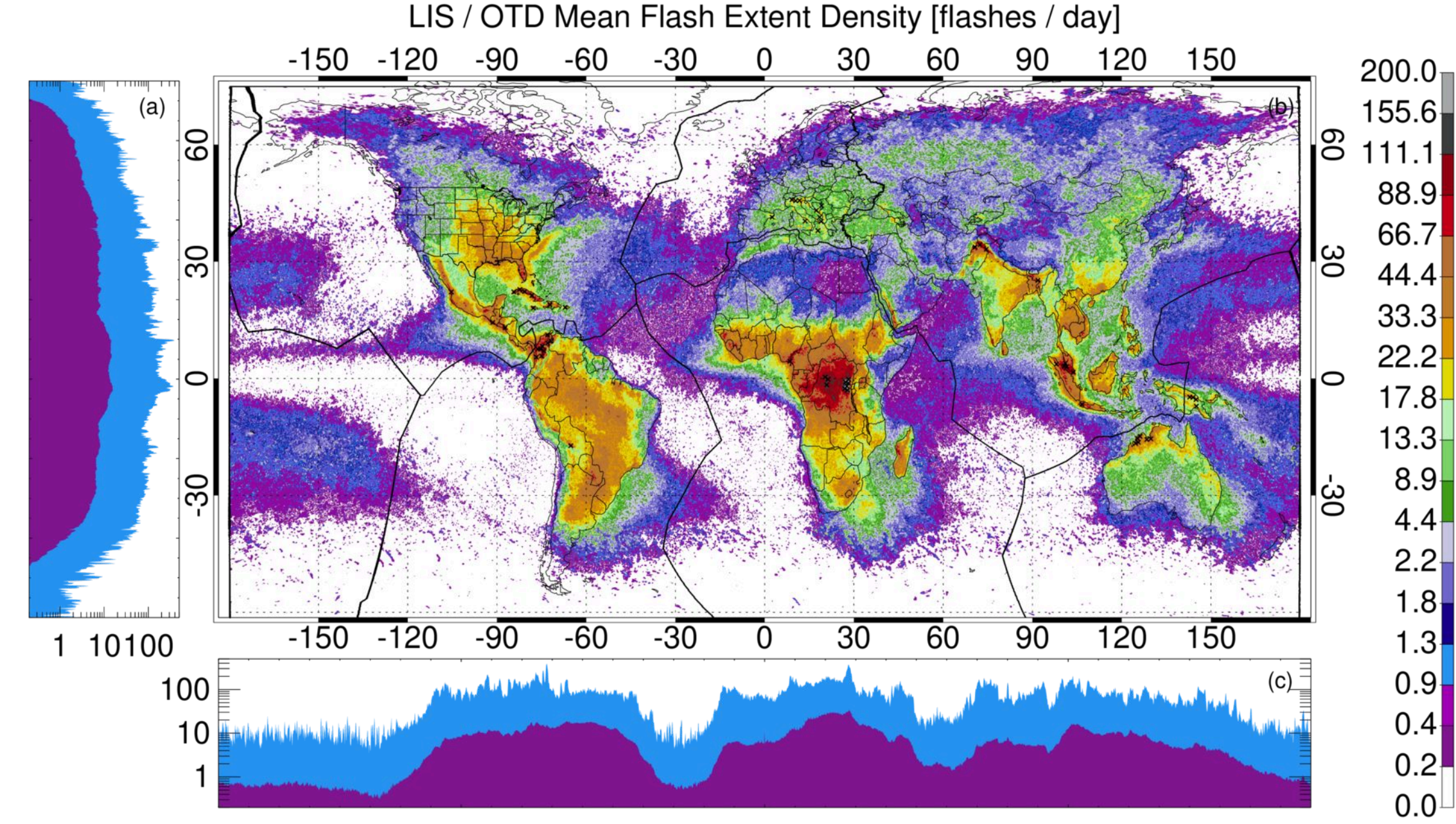
LIS / OTD Mean Flash Extent Density [flashes / day]
(a)
1 10100
-150 -120 -90 -60 -30 0 30 60 90 120 150
60
30
0
-30
(b)
(c)
100
10
1
200.0
155.6
111.1
88.9
66.7
44.4
33.3
22.2
17.8
13.3
8.9
4.4
2.2
1.8
1.3
0.9
0.4
0.2
0.0

Figure 8.

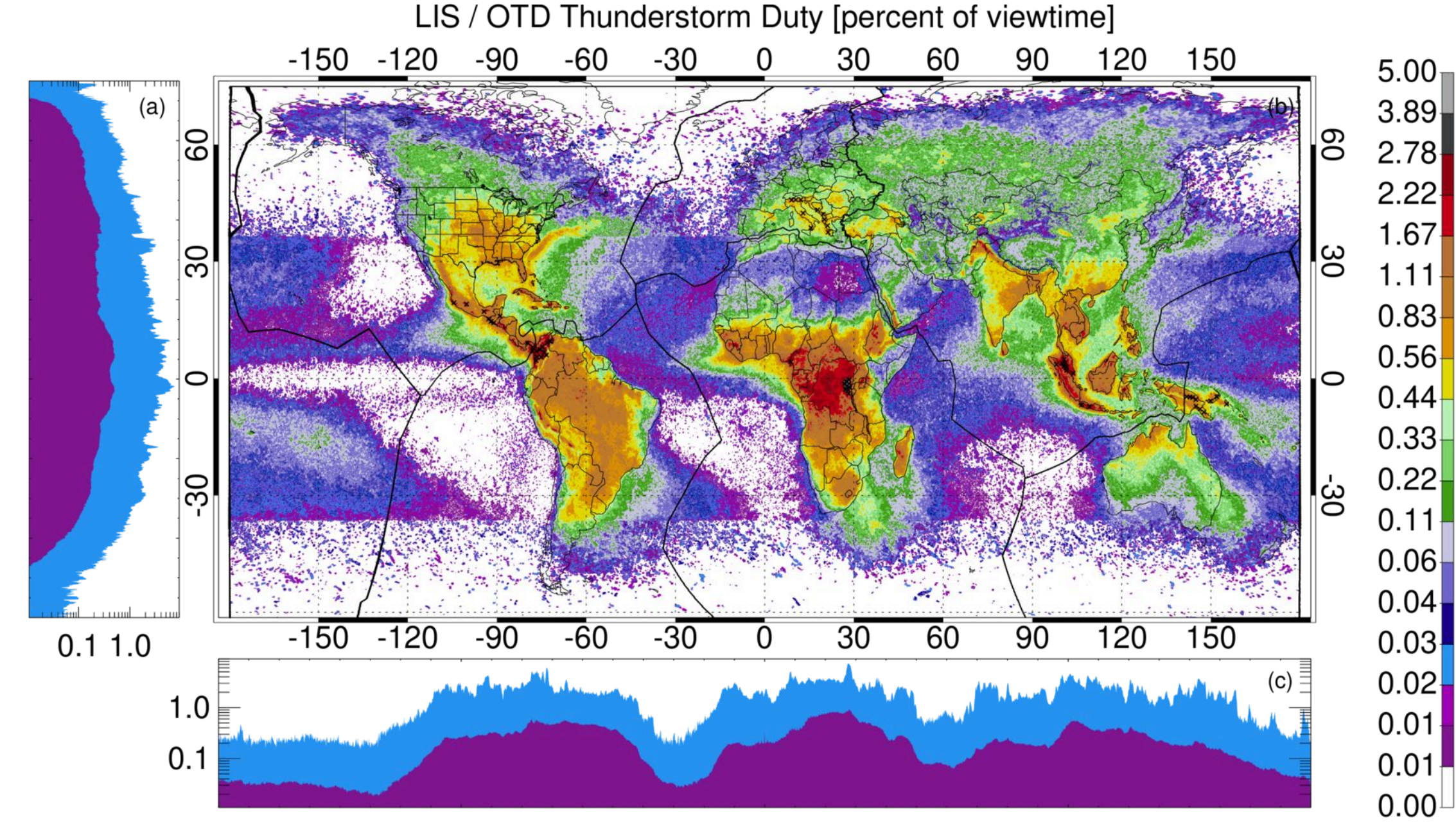
LIS / OTD Thunderstorm Duty [percent of viewtime]
(a)
0.1 1.0
(b)
-150 -120 -90 -60 -30 0 30 60 90 120 150
60
30
0
-30
(c)
1.0
0.1
5.00
3.89
2.78
2.22
1.67
1.11
0.83
0.56
0.44
0.33
0.22
0.11
0.06
0.04
0.03
0.02
0.01
0.01
0.00

Figure 9.

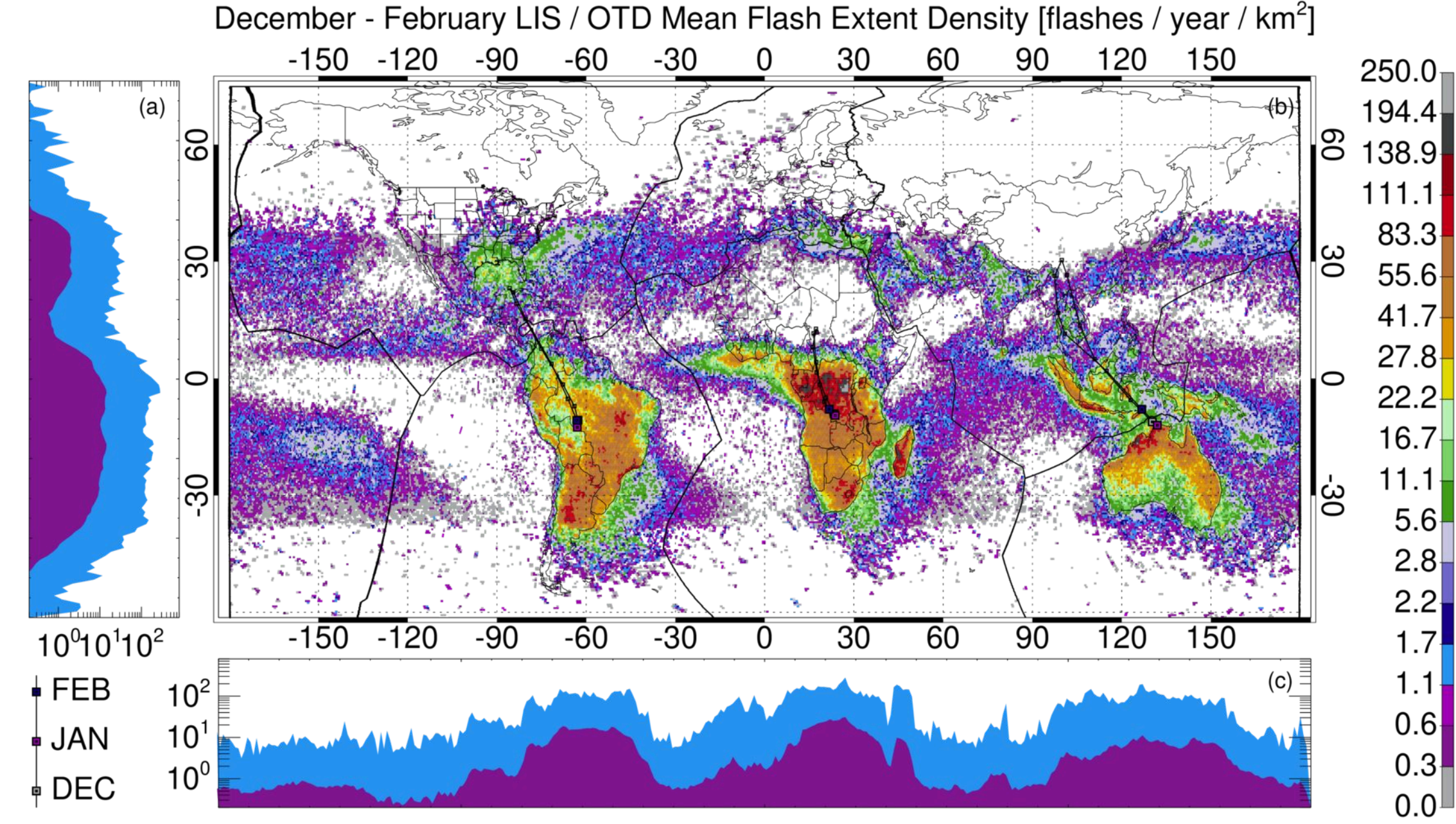
December - February LIS / OTD Mean Flash Extent Density [flashes / year / km^2]
(a)
(b)
(c)
-150 -120 -90 -60 -30 0 30 60 90 120 150
60
30
0
-30
10^0 10^1 10^2
FEB
JAN
DEC
250.0
194.4
138.9
111.1
83.3
55.6
41.7
27.8
22.2
16.7
11.1
5.6
2.8
2.2
1.7
1.1
0.6
0.3
0.0

Figure 10.

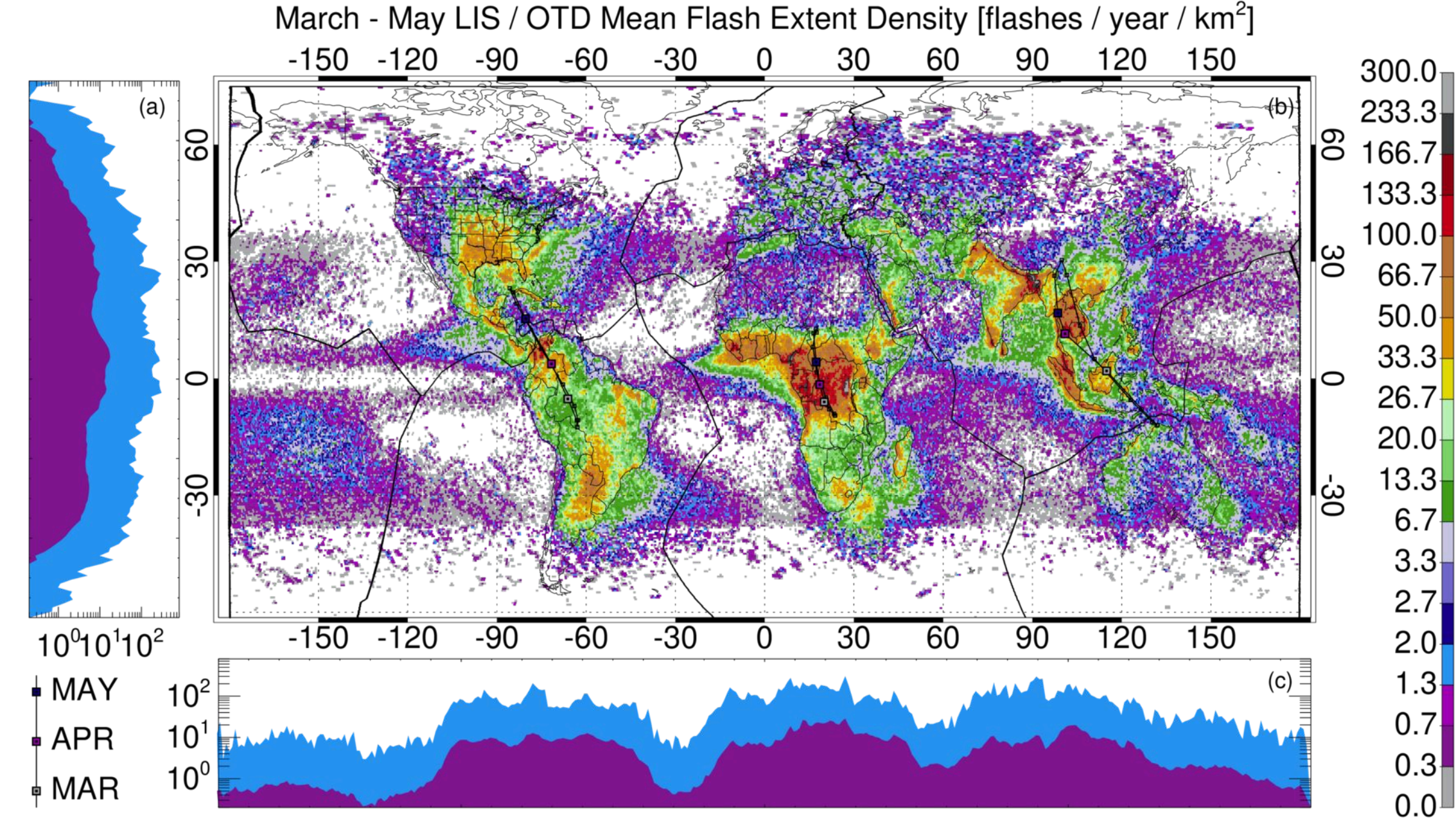
March - May LIS / OTD Mean Flash Extent Density [flashes / year / km^2]
-150 -120 -90 -60 -30 0 30 60 90 120 150
60
30
0
-30
(a)
(b)
(c)
10^0 10^1 10^2
MAY
APR
MAR
10^2
10^1
10^0
300.0
233.3
166.7
133.3
100.0
66.7
50.0
33.3
26.7
20.0
13.3
6.7
3.3
2.7
2.0
1.3
0.7
0.3
0.0

Figure 11.

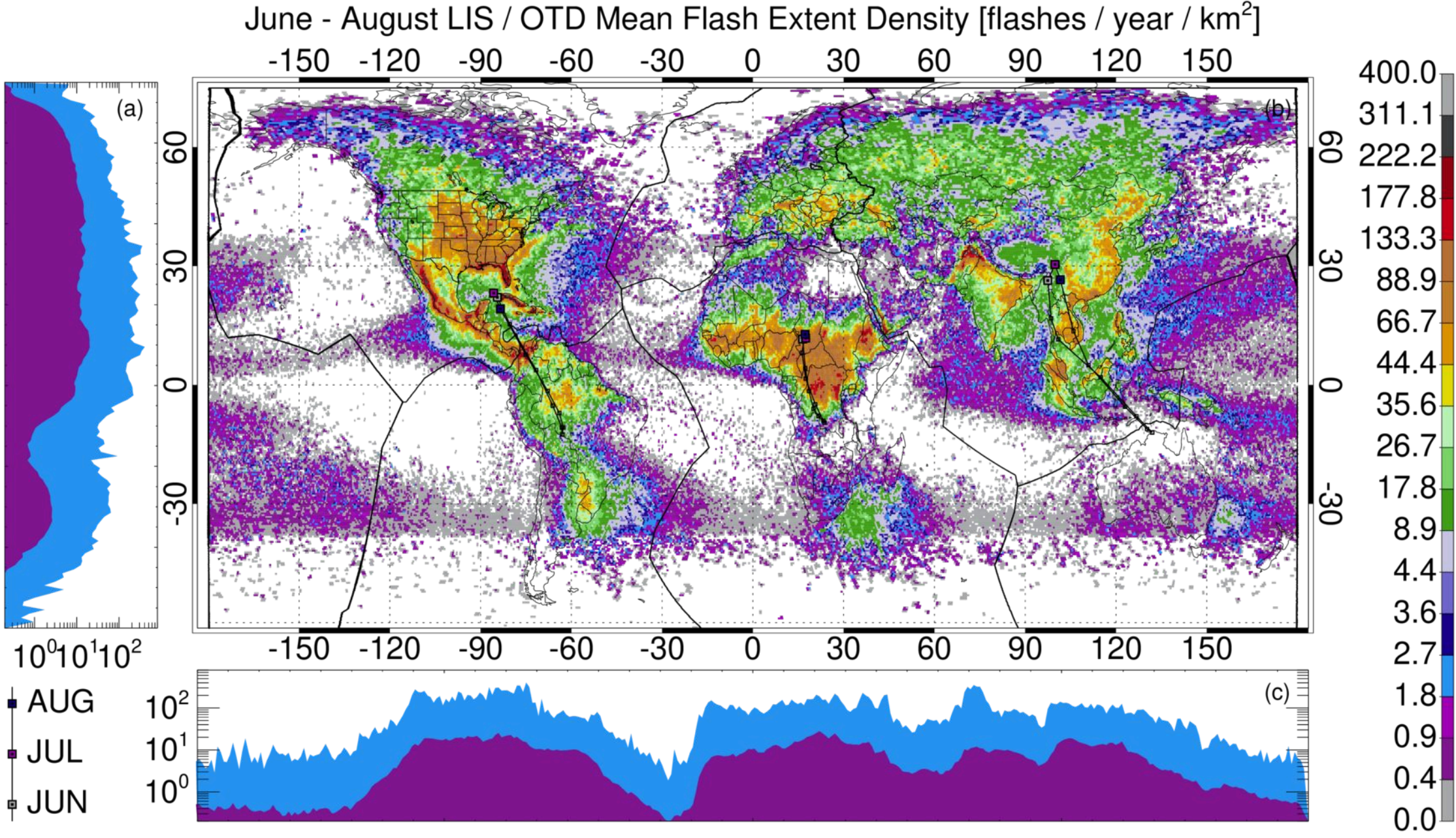
June - August LIS / OTD Mean Flash Extent Density [flashes / year / km^2]
(a)
(b)
(c)
-150 -120 -90 -60 -30 0 30 60 90 120 150
60
30
0
-30
10^0 10^1 10^2
AUG
JUL
JUN
400.0
311.1
222.2
177.8
133.3
88.9
66.7
44.4
35.6
26.7
17.8
8.9
4.4
3.6
2.7
1.8
0.9
0.4
0.0

Figure 12.

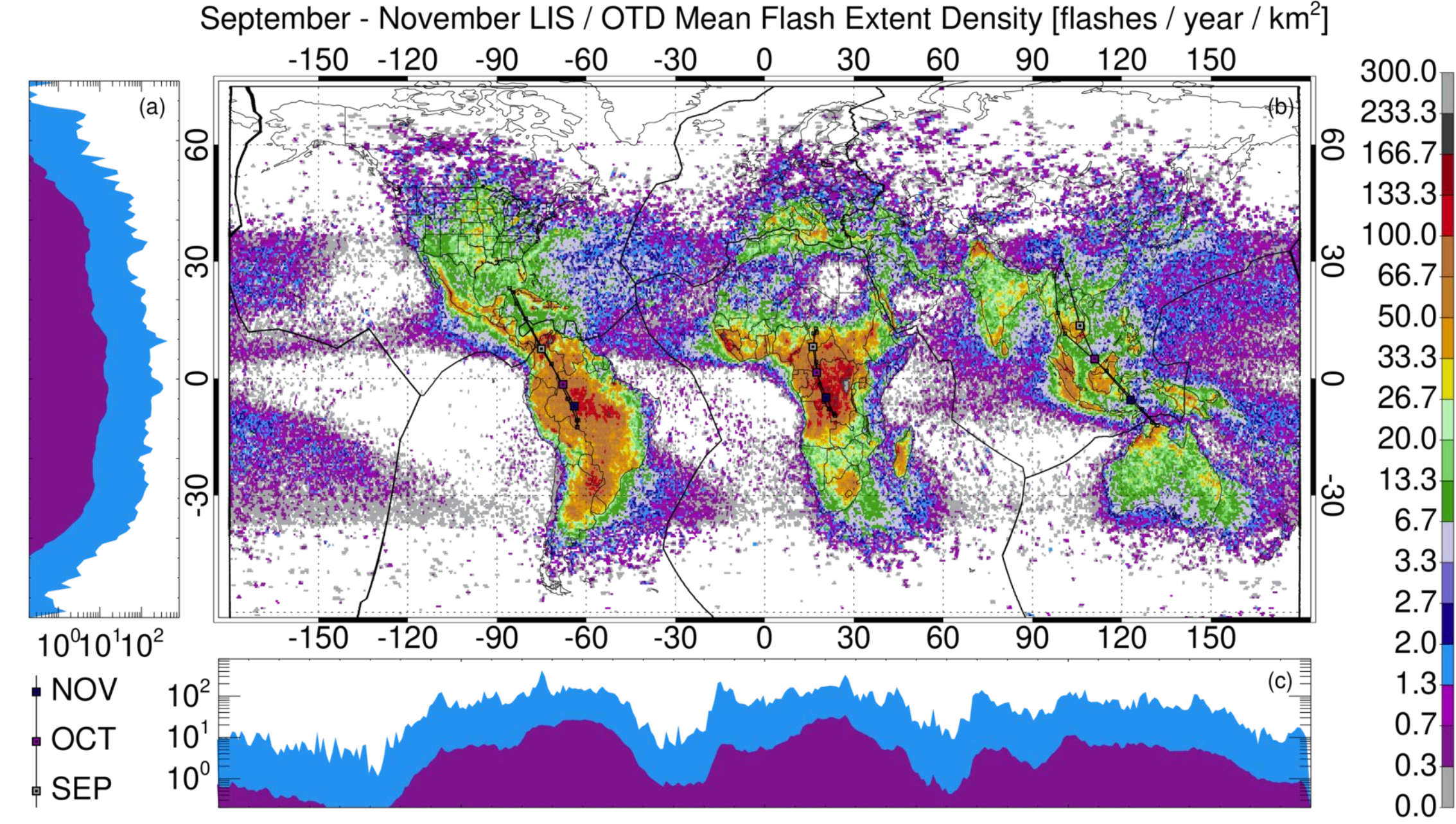
September - November LIS / OTD Mean Flash Extent Density [flashes / year / km^2]
(a)
(b)
(c)
-150 -120 -90 -60 -30 0 30 60 90 120 150
60
30
0
-30
10^0 10^1 10^2
NOV
OCT
SEP
10^2
10^1
10^0
300.0
233.3
166.7
133.3
100.0
66.7
50.0
33.3
26.7
20.0
13.3
6.7
3.3
2.7
2.0
1.3
0.7
0.3
0.0